NBSIR 80-2027

Measurement Techniques for Solar Cells, Annual Report September 15, 1977 to December 14, 1978

D. E. Sawyer, H. K. Kessler,
and H. A. Schafft

Electron Devices Division
Center for Electronics and Electrical Engineering
National Engineering Laboratory
National Bureau of Standards
U.S. Department of Commerce
Washington, D.C. 20234

July 1980

Prepared for
Department of Energy
Division of Distributed Solar Technology
Advanced Materials R&D Branch
Under Task Order AO54-SE of
Interagency Agreement EA-77-01-6010

NBSIR 80-2027

MEASUREMENT TECHNIQUES FOR SOLAR CELLS, ANNUAL REPORT SEPTEMBER 15, 1977 TO DECEMBER 14, 1978

D. E. Sawyer, H. K. Kessler,
and H. A. Schafft

Electron Devices Division
Center for Electronics and Electrical Engineering
National Engineering Laboratory
National Bureau of Standards
U.S. Department of Commerce
Washington, D.C. 20234

July 1980

Prepared for
Department of Energy
Division of Distributed Solar Technology
Advanced Materials R&D Branch
Under Task Order AO54-SE of
Interagency Agreement EA-77-01-6010

U.S. DEPARTMENT OF COMMERCE, Philip M. Klutznick, *Secretary*

Luther H. Hodges, Jr., *Deputy Secretary*
Jordan J. Baruch, *Assistant Secretary for Productivity, Technology, and Innovation*

NATIONAL BUREAU OF STANDARDS, Ernest Ambler, *Director*

Measurement Techniques for Solar Cells, Annual Report
September 15, 1977 to December 14, 1978

D. E. Sawyer, H. K. Kessler, and H. A. Schafft

Table of Contents

LIST OF FIGURES

Page

PREFACE

This work was conducted as a part of the Semiconductor Technology Program of the National Bureau of Standards (NBS). This program serves to focus NBS research to enhance the performance, interchangeability, and reliability of integrated circuits and other semiconductor devices including solar cells through improvements in measurement technology for use in specifying materials and devices in national and international commerce and for use by industry in controlling device fabrication processes. This research leads to carefully evaluated and well-documented test procedures and associated technology. Special emphasis is placed on the dissemination of the results of the research to the appropriate technical community. Application of these results by industry will contribute to higher yields, lower cost, and higher reliability of semiconductor devices. Improved measurement technology also leads to greater economy in government procurement by providing a common basis for the purchase specifications of government agencies and, in addition, provides a basis for controlled improvements in fabrication processes and in essential device characteristics.

The work reported herein was supported by the Division of Distributed Solar Technology of the Department of Energy (DOE) under DOE Task Order A054-SE of Interagency Agreement EA-77-A-01-6010. The task order is monitored by the SERI Photovoltaics Program Office (PVPO), Dr. Donald L. Feucht, Chief. The NBS point of contact for information on the various task elements of this project is Harry A. Schafft of the Electron Devices Division in the NBS Center for Electronics and Electrical Engineering.

The objectives of the work are to support the PVPO photovoltaic effort in the following ways:

1. By developing solar cell device and material measurement techniques using the laser flying-spot scanner originally developed at NBS for use on integrated circuits and discrete transistors, and

2. By assisting DOE in organizing and hosting appropriate workshops and symposia, and by providing general consultation and liaison services.

Disclaimer

Certain commercial equipment, instruments, or materials are identified in this report in order to adequately specify the experimental procedure. In no case does such identification imply recommendation or endorsement by the National Bureau of Standards, nor does it imply that the material or equipment identified is necessarily the best available for the purpose.

Measurement Techniques for Solar Cells, Annual Report
September 15, 1977 to December 14, 1978

D. E. Sawyer, H. K. Kessler, and H. A. Schafft
Electron Devices Division
National Bureau of Standards
Washington, DC 20234

1. Executive Summary

This report covers research performed in the period September 15, 1977 to December 14, 1978 under the program Solar Cell Measurement Technique Development and Other Services by the Electron Devices Division of the National Bureau of Standards. The objectives of this project are to provide support to the Department of Energy (DOE) thin-film photovoltaic effort in the following ways: (1) by developing solar cell device and material measurement techniques using the NBS-developed laser flying-spot scanner and (2) by assisting the DOE in organizing and hosting appropriate workshops and symposia and providing general consultation and liaison services.

In this annual report, many applications of the laser scanner are described, and others are proposed. The laser scanner itself is described in Appendix A. The applications described include detecting cell cracks, determining metallization "breaks," and locating metallization regions making poor ohmic contact with the underlying emitter surface. Preliminary work on gallium arsenide metal-insulator-semiconductor (GaAs MIS) cells indicates that the scanner can identify portions of a cell which are less effective than others due to "island formation," i.e., break-up of the thin, optically transparent metal film, which may occur in these structures. The scanner can also provide information useful to the cell designer.

At the outset of the work it was thought that information such as that enumerated above could only be obtained by scanning with light modulated at microwave frequencies, but a technique much simpler than this was conceived and successfully developed. It employs forward biasing of the cell during scanning. Forward bias may be provided by use of an illumination source, by an externally supplied current source, or by a combination of the two. The scanning technique is nondamaging; it requires no electrical contacts to the cell other than those already present, and it can be used on encapsulated or unencapsulated cells in almost any laboratory or test environment.

The case of scanning between parallel emitter metallization stripes using a line of light was analyzed for two cases: (1) a reverse-biased cell illuminated with the light modulated at microwave frequencies and (2) a forward-biased cell illuminated with unmodulated light. The mathematics is similar for both situations. For the

latter, the maximum-to-minimum cell response signal ratio* depends only on the emitter sheet resistance, the stripe separation, and the cell conductance per unit area; the last can be varied by adjusting the cell current. The analysis predicts that the emitter sheet resistance can be obtained by fitting the analytical value for the maximum-to-minimum ratio to the experimentally observed ratio. Drs. K. Lehovec and A. Fedotowsky, working under subcontract at the University of Southern California, extended the mathematical analysis and cell modeling effort to include the use of a scanning light spot on more realistic cell geometries than the one-dimensional case described above.

The results of the in-house device modeling work and mathematical analysis outlined above were used to develop the specifications required of a high-intensity light source for cell biasing during laser scanning. This source was subsequently constructed and successfully employed.

Before this program began, the laser scanner had been used primarily for ICs and other transistor-like devices. To obtain optimum conditions for scanning solar cells, several modifications were made to the scanning apparatus, and ancillary equipment (including the light source mentioned above) was designed and constructed. Optical elements were acquired to allow the raster scanning region to be increased from a previous maximum area value of 3 mm (0.12 in.) square to an area as large as 100 mm (4 in.) square. A vacuum hold-down and rocking stage were fabricated (the rocking feature is needed when one desires reflected-light information). A simple but effective jig was designed and constructed to permit each of the 36 5.7-cm (2.25-in.) diameter cells in a 25.4-cm (10-in.) by 61-cm (24-in.) module to be scanned while biased to reveal cell defects. A means was developed to couple forward-biased, and consequently low-impedance, scanned cells to the display electronics without degrading the cell's inherent signal-to-noise ratio and video information content.

The design of a mask set for a reference structure array (RSA) was completed. The results of measurements on these RSAs will be used to verify the validity of using the mathematical modeling work, including the presence of various types of cell defects, to quantify the results of laser scanning experiments. The objective of this verification is to put the laser scanning techniques for solar cells on a firm analytical basis. The RSA consists of four solar cells, each surrounded by test patterns to give a mean value of, and the spatial variation in, the following: cell and material properties and parameters (including emitter and metallization sheet resistance), metal-to-emitter contact resistance, substrate resistivity, and carrier density in the base as a function of distance below the emitter-base junction. The first solar cell contains no intentional defects; the second contains emitter metallization stripes with

*Response adjacent to metallization to response at mid-distance to next parallel metallization stripe.

"open" regions of various controlled sizes; the third has no opens, but does have an emitter sheet resistance which varies periodically in a stripe pattern; and the fourth contains both opens and the emitter sheet resistance variation described above. The RSAs will be made from single-crystal silicon at the NBS fabrication facility; only silicon technology offers the fabrication precision required.

A workshop on the Stability of (Thin Film) Solar Cells and Materials was conducted at the National Bureau of Standards on May 1 to 3, 1978 as part of the Department of Energy's National Photovoltaic Program. The workshop program is included as Appendix B. The workshop addressed many of the problems and obstacles to achieving stability and long life of terrestrial solar cell devices using advanced technology. The following three groups of exploratory solar cell materials and concepts were considered: (1) Cu_2S/[CdZn]S, Cu-Ternaries/CdS, CdS/InP, and amorphous Si; (2) polycrystalline Si, MIS, and conducting oxide Si; and (3) polycrystalline and AMOS GaAs.

During this reporting period, plans were initiated for a workshop on photovoltaic material and device measurements, scheduled to be held in the Washington, D.C. area in the spring of 1979. The purpose of the workshop is to accelerate the development of thin-film solar cells by improving the versatility and reliability of material and device measurement techniques. The preliminary plans for the workshop are included as Appendix C.

The publications and talks associated with the work conducted in this reporting period are listed in Appendix D.

2. Applications of the Laser Flying-Spot Scanner to Solar Cells

2.1 Overview of Some Cell Problems

The requirements placed on terrestrial solar cells developed for DOE's Photovoltaic Program are unique in that the combination of adequate efficiency, low cost, and long life is demanded. Satisfying this set of requirements means that some serious problems have to be faced and overcome. Some of the cell types that are leading contenders for wide-spread deployment may be made from poorly understood materials by inadequately controlled and understood fabrication techniques. History has shown that these inadequacies can sometimes lead to periods of cell production during which cell performance is inexplicably poor.

An alternate approach to satisfying DOE's requirements is to use small amounts of relatively expensive but well-understood materials such as single-crystal silicon or gallium arsenide, and rely on low-cost reflectors or Fresnel lenses to collect and focus the sunlight on the cell with concentration ratios of up to several thousand. The adequate design of a concentrator solar cell can be a formidable problem. An appropriate analysis would begin with a device model suitable for computer simulation in three dimensions where the device parameters values could vary over this space. There are disadvantages to this approach, however. One is that the comprehensiveness of the model could obscure the cause and effect relationships between device parameter values chosen and overall cell efficiency. That is, the possible usefulness of the computer results in predicting what should be done to improve the cell may be obscured by the many quantities one could vary; it is not known on an *a priori* basis which quantities are important and must be specified accurately, and which quantities may safely be neglected for the sake of simplicity, to obtain a solution which may lead to better design insight.

A third important class of cells, nonconcentrator types made from single-crystal materials, is fabricated by techniques which are quite similar to those developed by the integrated circuit industry. The solar cell emitter region (that portion above the p-n junction) is quite thin to enhance the cell response in the blue region of the spectrum, typically less than half a micrometer in the more recent efficient designs. The thinness of the emitter makes it difficult to fabricate uniform, low-resistance contacts to the emitter without having the metallization short circuit the junction.

The laser flying-spot scanner can be applied to aid in overcoming many of the above problems. Ways in which the scanner can be so used are reported in this document.

2.2 Spatial Variation of Cell Response

It would be extremely useful, especially for concentrator cells, if one could measure the spatial uniformity of the cell response over its surface. This could provide one check of the cell's design and fabrication steps. The scanner has been used in a rather simple manner to do this. It has been used to reveal those portions of a cell which are not as effective as other parts in producing load power under illumination. Furthermore, it presents this

information in a quantitative manner so as to allow an accurate assessment of the cell deficiencies. This is a straightforward scanner application. The technique described in this report can be used for any cell composition; it provides information badly needed for concentrator cell design and assessment. It can also be used to obtain a better understanding of the behavior of nonconcentrator cells, both of the conventional p-n junction single-crystal variety and those made using structures and materials of a more exploratory nature.

The technique itself is very simple. The cell is scanned with a spot of light while it is uniformly illuminated by a bias light that can be increased step-wise in intensity. By self-biasing the cell with light, one can simulate operation in the field. For some cell types, one may also provide cell biasing by means of an externally imposed electrical current source and achieve equivalent scanning results. Under these conditions, the scanner display screen presents a map of the small-signal, or incremental, cell response. By scanning the cell under various loads between zero ohms (the cell termination for measurement of short-circuit photocurrent) and infinity (the cell termination for measurement of open-circuit photovoltage), one can obtain maps which when compared to each other show the load-to-load variation of the photoresponse over cell. The maps can further be interpreted to yield desired information about the cell's point-to-point operation. These biasing techniques, and the scanning results obtained, are discussed in section 4.

Prior to the present reporting period, experiments were made on reverse-biased p-n junction diodes scanned with light modulated at microwave frequencies to reveal the diode's passive and distributed nature. This work is included in the next section to serve as an introduction to the present, more convenient, scanning technique. The present technique uses cell dc forward biasing, and unmodulated scanning light,* to reveal not only the passive nature, e.g., emitter sheet resistance, metallization defects, etc., but also the active nature of the cell.

*For purposes of this report, "unmodulated scanning light" may also include light modulated at frequencies well above those contained in the waveform of the cell's normal response to scanned unmodulated light.

3. Early Laser Scanning Work Using Light Modulated at Microwave Frequencies

The photomicrograph in figure 1a shows the silicon chip used for the first laser scanning observations of emitter lateral (sheet) resistance. There are nine diodes, each about 250 μm on a side, formed by an *n*-type planar diffusion into *p*-type silicon of about 5-Ω•cm resistivity to achieve a junction depth of about 1 μm. These values of junction depth and bulk resistivity are close to those used for commercial silicon solar cells. Conventional techniques were used to bond the nine-diode chip to a header and to make a wire bond connection between one of the two ohmic contacts on the central diode and a header post terminal.

The other photographs in figure 1 are of the scanner display screen showing the photoresponses of the central diode due to its being scanned with laser light of wavelength 0.633 μm while a reverse voltage of 5 V is applied to the diode. The photoresponses are presented as a superposition of an intensity modulated signal (conventional z-axis mode) and a vertical deflection signal.

Figure 1b is a photograph of the diode's response to unmodulated light. Figure 1c shows the response of the diode to a 500-MHz modulated component superimposed on the unmodulated light while the bias conditions are maintained. Figure 1d is the corresponding response to a 1.0-GHz modulation. The gain of the display screen was adjusted to maintain the same maximum vertical deflection in all three photographs. This maximum occurs when the scanning spot is located at the edge of the bonded contact. It is seen that the 500-MHz and 1.0-GHz photoresponses from the portions of the diode away from the bonded contact decrease as the modulation frequency increases and as the distance from the contact increases.

Figure 2 can be used to explain the results shown in figure 1. Figure 2a is a cross section through the diode, and figure 2b is the corresponding one-dimensional electrical representation of the diode. The diffused emitter region is represented by a distributed resistor and the junction transition region by a distributed capacitor. One would expect such a network to behave in the manner observed: the signal to the radio receiver would decrease with increasing signal frequency and with increasing distance of the laser excitation from the bonded contact, as sketched in figure 2c, because the attenuation due to the distributed resistance-capacitance line increases with these quantities.

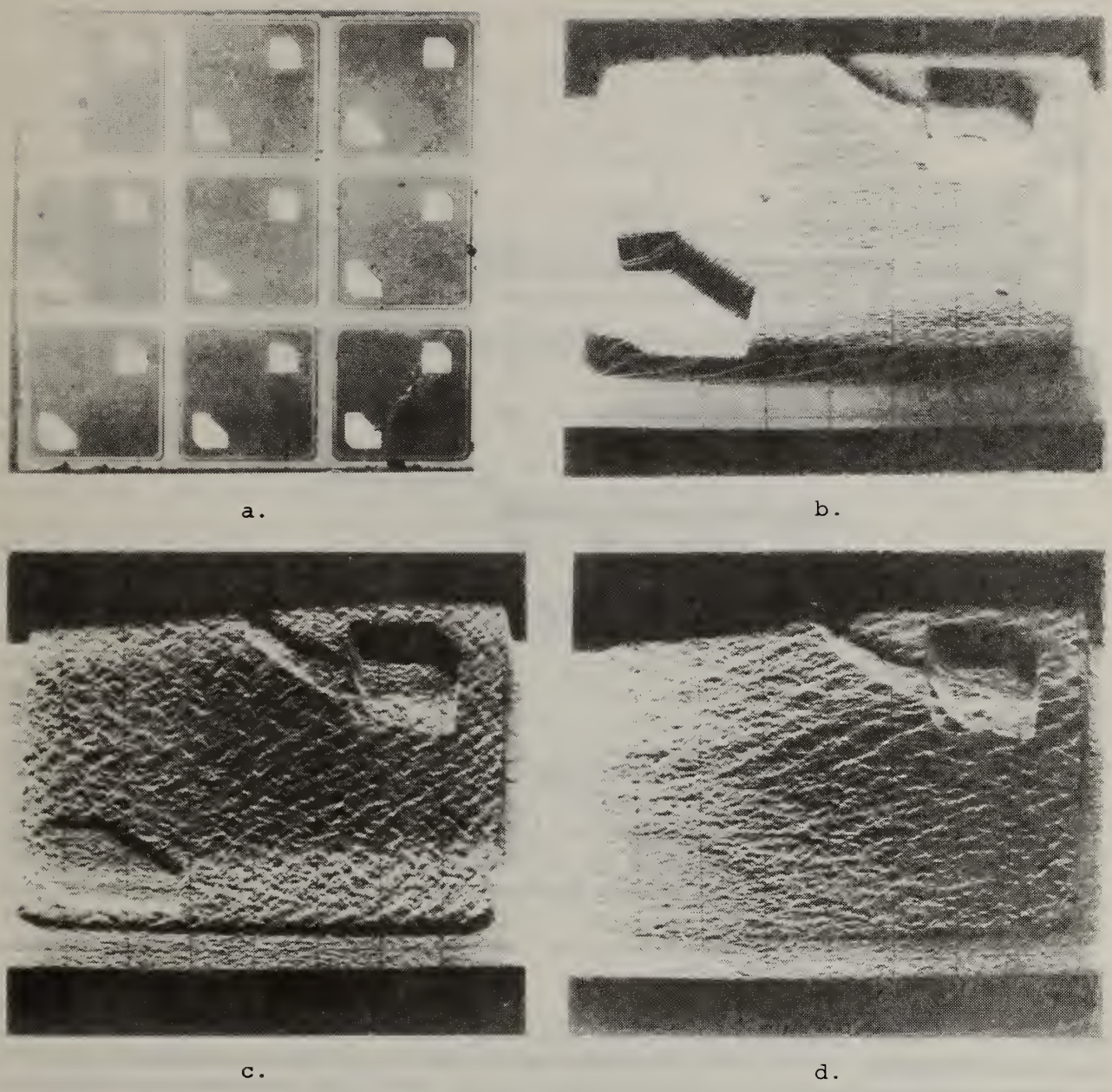

Figure 1. Silicon p-n junction diode photoresponse. (a) Photomicrograph of diode array; the diode scanned is the central one in the array. (b) Photoresponse to unmodulated 0.633-μm light and with the diode reverse biased 5 V. (c) Photoresponse for the same conditions except that the screen now displays the diode response to the light component modulated at 500 MHz. (d) Same as (c) except the modulation frequency is 1.0 GHz.

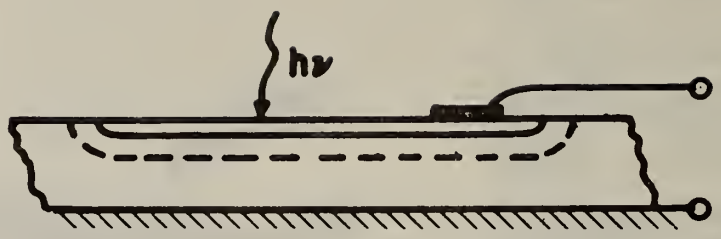

a.

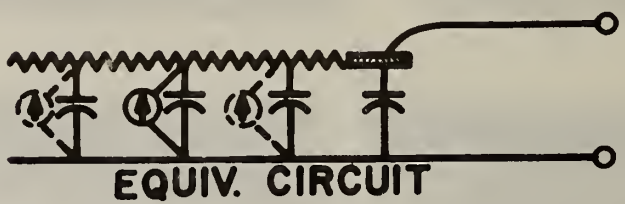

b.

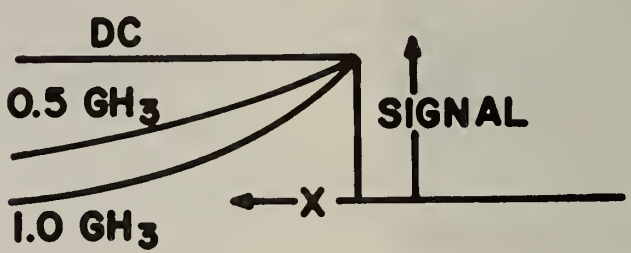

c.

Figure 2. A model relating the diode scanning results shown in figure 1 to the diode geometry and electrical characteristics. (a) Cross-sectional view of diode (not to scale). (b) Equivalent circuit of diode. (c) Photoresponse to 0.633-μm unmodulated light and 0.633-μm light modulated at 0.5 and 1.0 GHz.

4. Development of Solar Cell Device and Material Measurement Techniques

4.1 Cell Scanning Technique Employing Light and Current Source Cell Biasing

A new method was conceived to detect and study cell faults, such as regions of poor metallization, and to determine important cell parameters such as emitter sheet resistance. This method was applied to a variety of cell types and the basic soundness of the method was confirmed.

The method makes use of a cell's distributed nature when it is forward biased, bias conditions similar to those which exist when a solar cell is exposed to sunlight. Unmodulated scanning light is employed. The scanning light source most often used is a low-power (3-mW) continuous wave helium-neon laser operating at 0.633 μm. Also used is a laser operating at 1.15 μm. The effect of scanning a solar cell with a light spot is to place a signal current source across the cell barrier, e.g., the p-n junction, at the point illuminated by the spot. The bias may be provided by either exposing the cell to light, or by connecting the cell to an external electrical current source, or by a combination of these two means. The results of calculations, which have been confirmed by measurements, show that the cell currents required to display the desired scanner information are comparable to those which normally occur within the cell when the cell is exposed to irradiance levels for which it was designed.

The new method allows one to detect potentially harmful cell cracks with a sensitivity greater than any previously reported method. It also allows one to locate regions of cell emitter metallization which are either broken or not in good ohmic contact with the underlying emitter. The method is much easier to employ than the originally envisioned scheme in which a reverse-biased cell is illuminated with light modulated at microwave frequencies. Other attributes of the method are: it is nondamaging, it requires no electrical contacts to the cell other than those already present, and it can be used on encapsulated or unencapsulated cells in almost any laboratory or test environment. A preliminary account of the method was given at the IEEE 13th Photovoltaic Specialists Conference [1], and a more complete description was made at the 1978 Report Session of the Advanced Materials R&D Branch [2].

4.1.1 Description of Technique

The low-frequency small-signal equivalent circuit of a biased and scanned cell is a three-dimensional resistive array. The scanning light spot is represented by a current generator moving within the array as the spot scans the cell. The array components are normally made up of the cell emitter sheet resistance and the distributed resistance for the p-n junction. This distributed resistance is the local slope of the voltage-current curve for each incremental cell area. A simplified, one-dimensional analysis of this array is presented in section 4.6.2. The highlights are given in this section.

The analysis proceeds in a manner similar to the one for light modulated at microwave frequencies presented in section 4.6.1; in the present case, the local voltage-current slope associated with the p-n junction plays a role similar to the distributed transition-region junction capacitance for the

case in which the light is modulated at microwave frequencies. Implementation of the newer technique is easier because high-frequency equipment and techniques are not needed.

Figure 3 is an end-on view, not to scale, of an idealized solar cell showing the portion between a contiguous pair of (parallel) metallization stripes, and figure 4 is its one-dimensional electrical representation for the case of scanning with a line of light. This type of scanning will probably not be performed in the program, but this case was used for analysis in section 4.6.2 because the solution can be obtained as a closed-form expression which may be examined to anticipate the important results for more realistic two-dimensional cases. In figure 4, the emitter is represented by the continuous resistive element, and the small-signal voltage-current ratios for the elemental diodes making up the cell between the stripes are represented by the discrete resistors connected with dotted lines. In the absence of significant shunting by the latter, the photocurrent will find its way to the load through one path or another. Thus, while the load voltage (the scanner display screen signal) may vary with light location due to spatial variations in such quantities as local lifetime, it will not be influenced by the proximity to a defect such as a region of poor metallization contact. In short, without significant internal shunting, the scanner is relatively insensitive to the detection of such cell defects such as cracks, regions of poor contacting, regions of excessive emitter sheet resistance, etc., which may seriously influence cell reliability and conversion efficiency.

The values of the shunt resistances can be varied by varying the diode forward bias. For the simple case in which all elemental diodes are equivalent and all are biased to the same voltage, the shunt conductance per unit area is the same for all portions of the cell. For σ_p representing this conductance, $\rho_\square$ representing the emitter sheet resistance, w and ℓ representing the metallization stripe length and separation, respectively, the voltage across the load Z_ℓ, i.e., the output voltage v_{out} for the scanning light line at the arbitrary position $0 \leq p \leq \ell$, is shown in section 4.6.2 to be

$$v_{out} = i_o Z_\ell \frac{\{\sinh[\beta(\ell - p)] + \sinh(\beta p)\}}{\left\{\sinh(\beta\ell) + \frac{2w\beta Z_\ell}{\rho_\square}[\cosh(\beta\ell) - 1]\right\}} , \tag{1}$$

where

$$\beta \equiv (\rho_\square \sigma_p)^{1/2} . \tag{2}$$

As the laser light line is swept from one grid stripe to another, v_{out} undergoes a maximum-minimum-maximum excursion where the ratio of minimum to maximum values is given by the following expression:

$$\frac{v_{out}(min)}{v_{out}(max)} = \operatorname{sech}(\beta\ell/2) . \tag{3}$$

Equation (3) is plotted in figure 5 for a representative value of $(\beta\ell/2)$. The desired forward biasing of the cell may be achieved by shining light on the cell. It is appropriate now to relate the shunt conductance σ_p to the cell current and associated air-mass-one (AM1) irradiance level. Figure 6

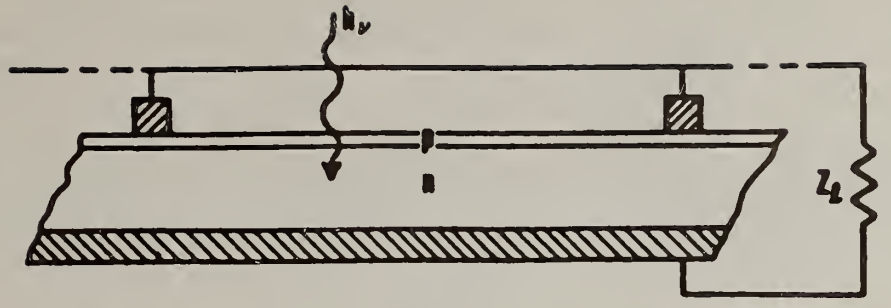

Figure 3. A cross section, not to scale, of an idealized solar cell connected to a load Z_ℓ, showing the portion between a contiguous pair of parallel metallization stripes.

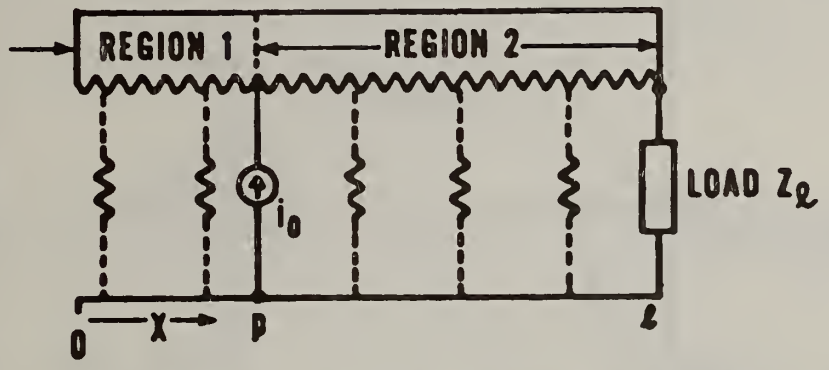

Figure 4. The one-dimensional electrical representation of figure 3 for the case of laser scanning with a line of light. The cell emitter is represented by the continuous resistive element, and the small-signal voltage-current ratios for the elemental diodes making up the cell between the stripes are represented by the discrete resistors shown connected with dotted lines and the line of light by an elemental current source.

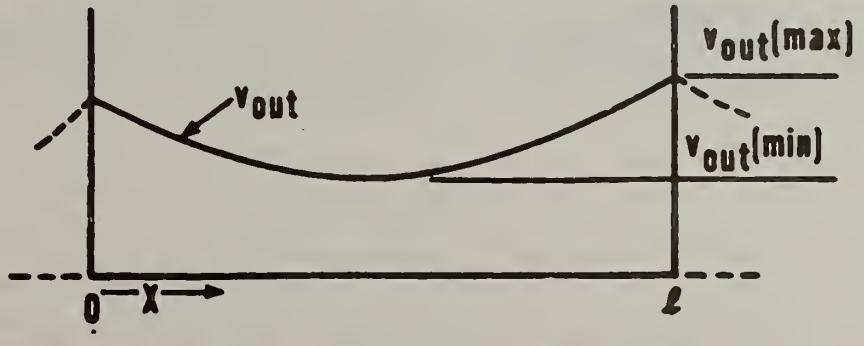

Figure 5. The variation of cell output voltage with scanning light position between parallel metallization stripes for a representative value of ($\beta\ell/2$) of 1.30.

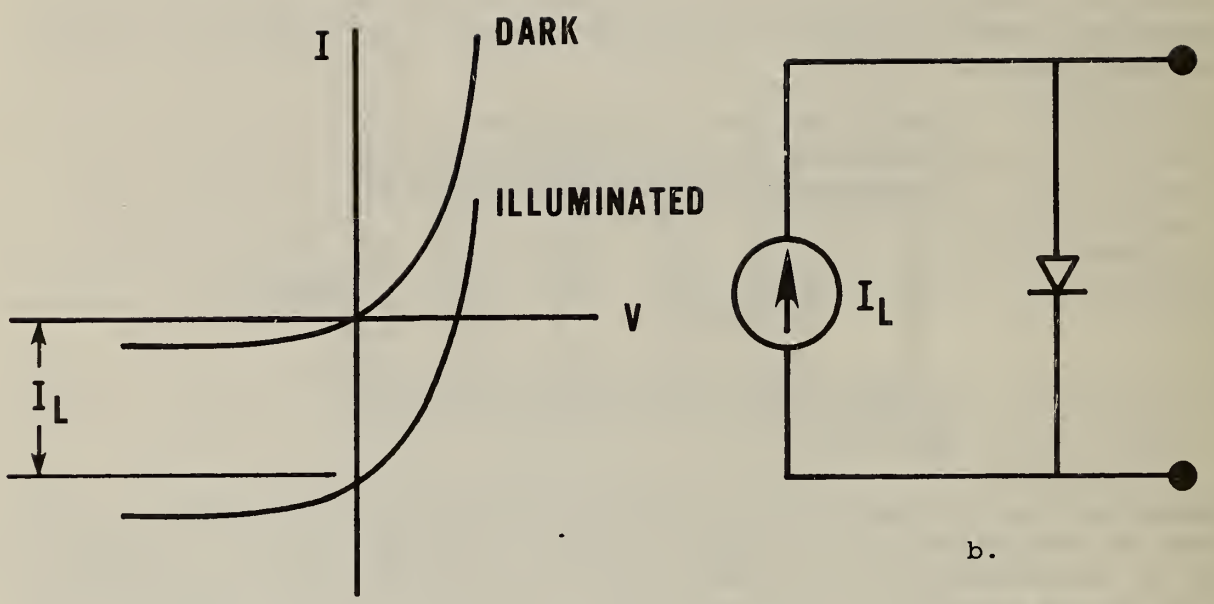

Figure 6. Idealized solar cell: (a) The I-V characteristics of the cell under both dark and illuminated conditions. (b) The equivalent circuit where the strength of the current generator is proportional to the illuminating light intensity.

shows the I-V characteristics for the dark and illuminated idealized solar cell and its equivalent circuit representation. The well-known effect of shining light on the cell is to displace the I-V characteristic along the I-axis an amount equal to the external current which would exist if the diode were connected to a short circuit. This current will be designated I_L. An alternate description states that charge flows through the cell in the forward-bias direction. For the idealized case discussed with uniform illumination, I_L is equal to the product of the cell junction area and the cell current density J_L due to illumination. In turn, J_L is related to the cell voltage V and J_o, the junction saturation-current density, by

$$J_L = J_o(e^{qV/kT} - 1) \quad . \tag{4}$$

In the scanning example described, the dc load to the cell is very large to approximate an open circuit condition and is illuminated by a constant light source while it is scanned with a much weaker (laser) source. The constant light source causes the cell to be forward biased and produces a small-signal junction conductance per unit area readily calculated by differentiating eq (4)

$$\sigma_p = dJ_L/dV = (q/kT)(J_L + J_o) \quad . \tag{5}$$

The current J_L will usually be several orders of magnitude larger than J_o, and so the quantity multiplying (q/kT) for all practical purposes is simply J_L. At room temperature, and with J_L expressed in amperes per unit area,

$$\sigma_p = 38.4\ J_L \text{ siemens per unit area} \quad . \tag{6}$$

The irradiance level for a representative cell and measurement condition can be readily calculated. Assume a stripe separation ℓ of 2 mm, an emitter sheet resistance $\rho_\square$ of 50 $\Omega/\square$, and 0.9 as the value of $v_{out}(min)/v_{out}(max)$ judged to just yield adequate scanning sensitivity. From eqs (2) and (3), the σ_p-value required for the assumed values of ℓ and $\rho_\square$ is 0.442 S/cm^2, and from eq (6), the required value of light-generated current is 11.5 mA/cm^2. The short-circuit photocurrent from a good quality silicon cell exposed to an an irradiance of one sun with an air-mass-one spectral distribution is about 38 mA/cm^2 [3]. The required cell irradiance level is approximately 0.30 suns, a value which can be reached quite easily in the laboratory. In figure 7, required irradiance levels are plotted *versus* desired scanning-sensitivity ratios for various combinations of stripe spacing and emitter sheet resistance. The irradiance values required to give the unambiguous v(min)/v(max) value of 0.5 for line-scanning typical nonconcentrator cell designs having ℓ-values from 1 to 3 mm and $\rho_\square$-values from 50 to 200 $\Omega/\square$ can be achieved with an irradiance source of 10 suns or less, according to this figure. Such an irradiance source has been constructed and is described in section 4.2.

The second way suggested to achieve internal resistive shunting, i.e., by using a current source, is conceptually simpler than flooding the cell with light. When an external current source is used, the cell emitter-base junction is no longer uniformily biased as when a uniform light source is employed, and no steady-state current exists in the cell load impedence. The equations presented in this section hold only for zero dc load-

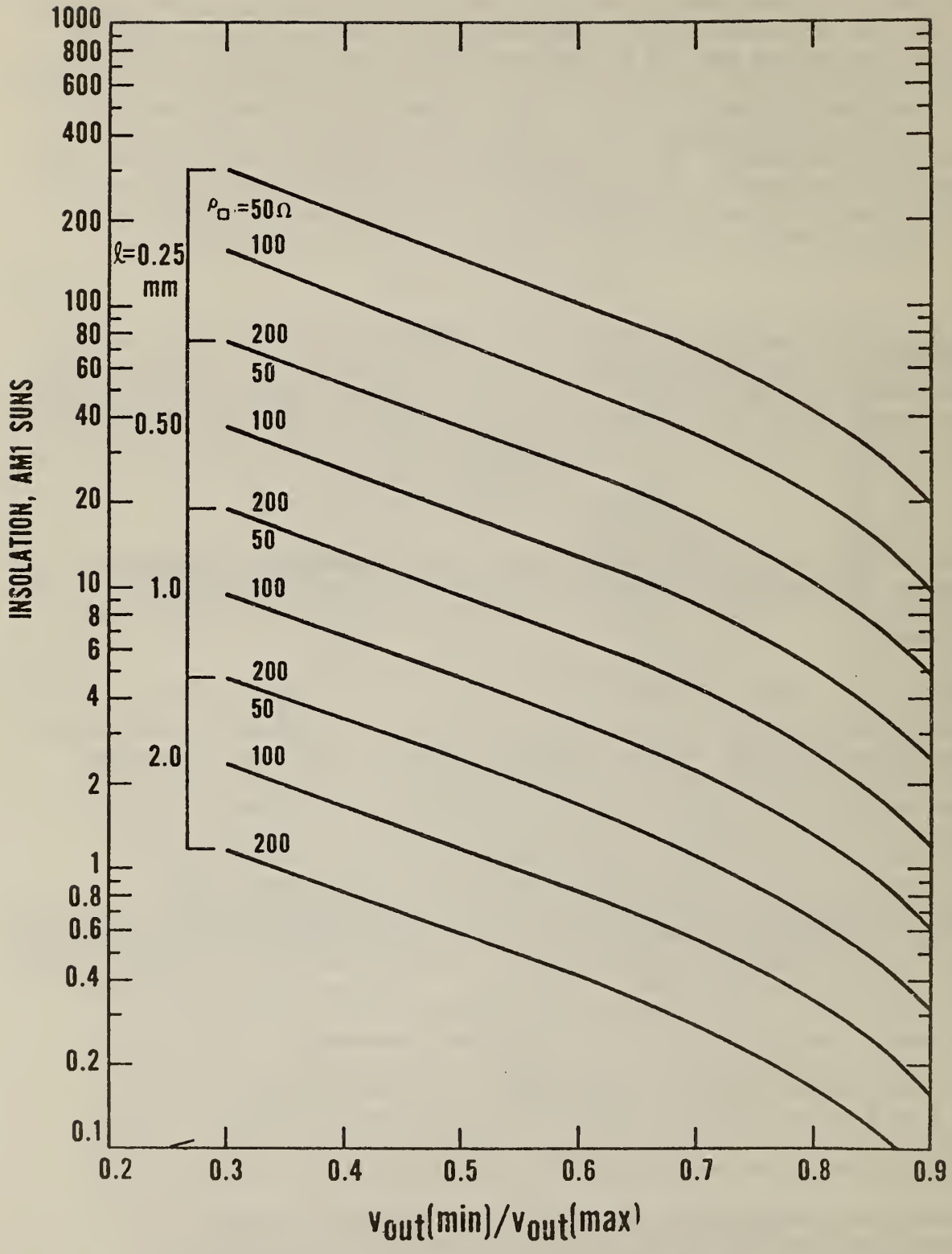

Figure 7. Air-mass-one insolation levels *versus* desired scanning-sensitivity ratios for various combinations of cell stripe spacing (ℓ) and emitter sheet resistance ($\rho_\square$) for a junction silicon solar cell.

current conditions, and an analysis of the case for an externally supplied electrical bias current is more complex. However, the cell scanning results discussed in the following section show that the method of using an external current source is a convenient way to detect a variety of cell defects.

4.1.2 Cell Scanning Results

4.1.2.1 Emitter Metallization Breaks

Results of scanning a space-flight quality solar cell are shown in figure 8 (with a sketch of the cell) and are used to demonstrate the detection of breaks in emitter metallization stripes. The cell was scanned while it was forward biased, either by light or by an external current source, or both.

Metallization breaks as detected with an optical microscope are shown by dots in the sketch. Because of the electrical redundancy in connecting the fine (50-μm wide) herringbone metallization grid lines in the central portion of the cell to the wide (280-μm) metallization splines, two breaks in a fine line are required to disconnect any appreciable length of fine-line metallization from the cell output electrode. The lower three photographs of figure 8 show the results of scanning with 0.633-μm laser light. No metallization defects are observed with the cell unbiased (fig. 8c). With the cell forward biased (figs. 8d and 8e), metallization defects are readily observed by the lowered photoresponse in the vicinity of the unconnected metallization. The metallization which is continuous to the splines appears to make uniform electrical contact to the underlying emitter, as evidenced by the photoresponse attaining a maximum adjacent to the metallization. In figures 8c and 8d, the horizontal scan lines are deflected upward by an amount proportional to the cell response to the scanning light spot. In figure 8e, the cell response is mapped in a more conventional manner, by modulating the display screen intensity. The photoresponse presentation is such that maximum screen darkness corresponds to maximum photoresponse. The resulting pattern outlines the metallization regions making effective contact between the cell emitter and output electrode. For both figures 8d and 8e, 360 mA of the cell current is provided by light and 126 mA by an electrical supply. Qualitatively, similar results were obtained with a more modest total cell current of 126 mA supplied by the electrical supply alone (this 126-mA value corresponds to about 80 percent of the cell short-circuit current were it exposed to AM1 insolation). The larger 486-mA bias current value was chosen to enhance the photographic presentation of the results shown in figures 8d and 8e. Even though scanning was performed with a spot of light, the general shape of the photoresponse *versus* position away from the broken metallization region is in qualitative agreement with the results predicted from the line-scan analysis performed in section 4.6.2 and with the generalized analysis in section 4.6.3.

4.1.2.2 Metallization Not in Ohmic Contact with the Emitter Region

The ability of the scanner to detect portions of the metallization not in ohmic contact with the emitter is demonstrated by the results of scanning an experimental polycrystalline silicon solar cell under development. The cell is about 3.3 by 3.3 cm (1.3 by 1.3 in.). It is encapsulated in a soft, transparent plastic which is about 0.25 cm (0.10 in.) thick at the surface.

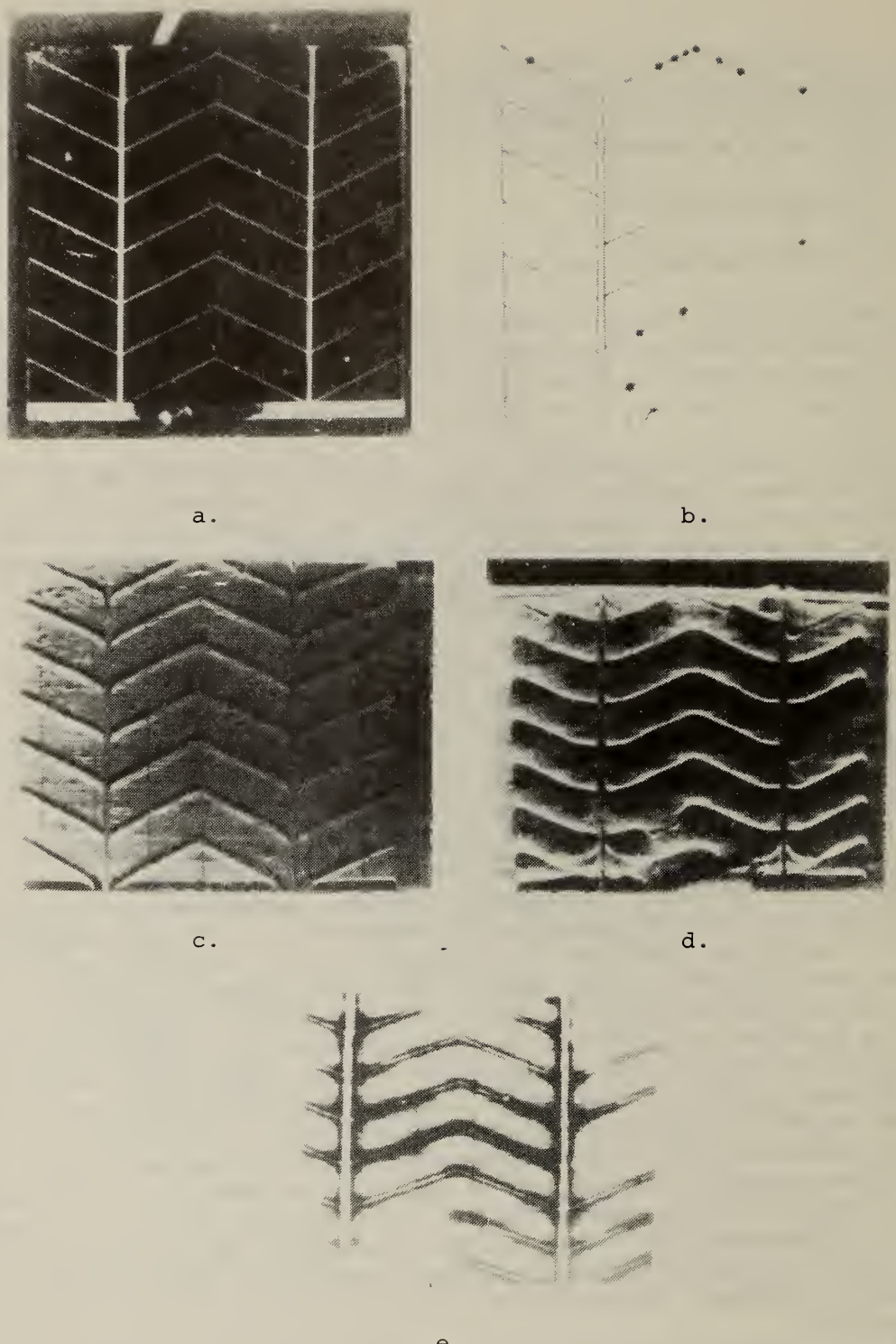

Figure 8. A 2- by 2-cm (0.8- by 0.8-in.) silicon "space" cell: (a) Photograph of the cell. (b) Sketch of cell with metallization breaks shown by dots. (c) Scanning photoresponse using the y-axis display mode and with the cell unbiased. (d) Scanning photoresponse using the y-axis display mode and with a cell bias of 486 mA. (e) Scanning photoresponse using the intensity-modulation display mode and with a cell bias of 486 mA.

A photograph of the cell is shown in figure 9a. The remaining photographs in figure 9 are of the display screen where the cell was scanned with 0.633-μm light. Figures 9b and 9c are for the cell with no bias applied and 9d and 9e are for the cell with a forward bias, supplied by an external current source of 100 mA. The intensity-modulation display mode is used in figures 9b and 9d, and the y-deflection display mode is used in figures 9c and 9e. It is sometimes desirable, as was done here, to use both these display modes separately. While the y-deflection mode is useful for quantifying cell defects, some portions of the cell response may block from view the response from other portions. By using the intensity-modulation mode first, one can view the response from all portions of the cell. The cell may then be repositioned, if necessary, for quantitative measurements of the photoresponse in the y-deflection presentation mode. One must be careful when comparing intensity-modulation mode photographs, however. Unless the photographs are made under identical electrical and photographic conditions, e.g., the same maximum signal excursions, the same "white level" signal values, the same film exposure times, etc., comparison of the photographs may be misleading.

The results shown in figure 9 indicate that although the top metallization is continuous to the output terminal, portions of this metallization are not making ohmic contact to the underlying semiconductor. This is evidenced by a lowered photoresponse on both sides of the metallization areas in question with the cell forward biased. This type of cell defect cannot be detected by previously available techniques such as optical inspection or laser scanning without bias.

In order for photoresponse at the edge of a solar cell metallization stripe to achieve a common, maximum value, the metallization must be continuous to the output lead and must make a uniform ohmic contact to the underlying semiconductor. These are precisely the fundamental requirements for effective metallization, and so the scanning technique described provides a test for cell metallization efficacy.

4.1.2.3 Cell Crack Detection

The biased-cell scanning technique was also used to locate cracks in solar cells. This is an important application because cracks have been known to cause cell arrays to fail, sometimes dramatically, with electric arcs and flames produced at the crack [4]. In order for a crack to be observed visually, it must be wide enough to scatter the observation light. For cells having a smooth surface, the width of the crack must be a fraction of a micrometer or wider. Solar cell cracks smaller than this, while not detectable, may widen in service. Cracks in cells with textured surfaces may be even harder to detect visually because the light reflected from the surface irregularities tends to obscure light scattered from the crack. These problems point to the need for a crack-detection technique which does not depend on visual inspection. Crack detection with the laser scanner makes use of the obvious consequence of cracking a semiconductor specimen: the electrical conductivity of a specimen becomes discontinuous at the crack. If the crack runs through the emitter of a solar cell, a discontinuity appears in the three-dimensional resistive array which represents the small-signal equivalent circuit of the cell in forward bias. This resistive discontinuity can be revealed by laser-scanning a forward-biased cell in the vicinity of the

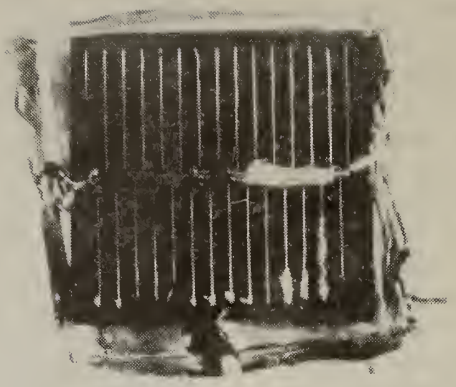

a.

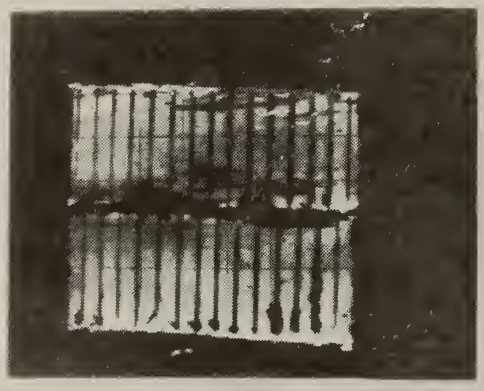

b.

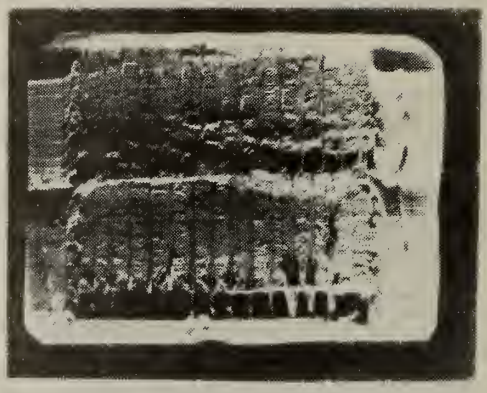

c.

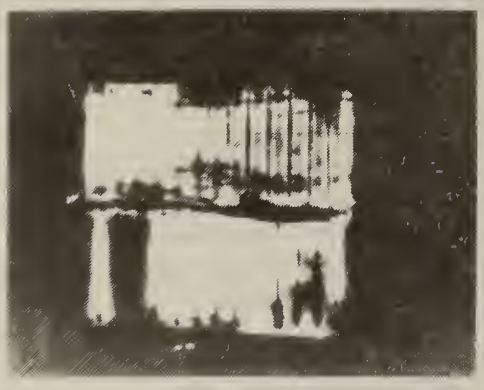

d.

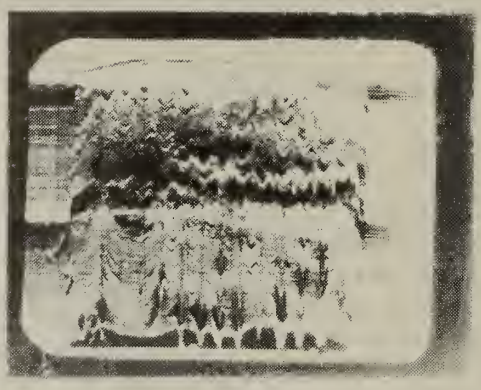

e.

Figure 9. A 3.3- by 3.3-cm (1.3- by 1.3-in.) polycrystalline silicon solar cell: (a) Photograph of the cell. (b) Scanning photoresponse using the intensity-modulation display mode and with the cell unbiased. (c) Scanning photoresponse using the y-axis display mode and with the cell unbiased. (d) Scanning photoresponse using the intensity-modulation display and with a cell bias of 100 mA. (e) Scanning photoresponse using the y-axis display mode and with a cell bias of 100 mA.

crack. One would expect resistive discontinuities to occur when the crack width is equal to or greater than the distance for majority-carrier tunneling, i.e., for cracks on the order of 2.5 to 10 nm wide or greater. Thus, scanning under proper conditions can reveal cracks 10 to 200 times narrower than can be observed under the most favorable conditions with visual inspection methods. It is not necessary for the scanning light spot diameter to be the same order of, or smaller than, the crack width. It is only necessary that the spot diameter be much less than the signal attenuation length, i.e., the distance over which the cell scanning response falls to e^{-1} of its maximum value. The attenuation length may be varied by adjusting the cell forward bias and is chosen typically to be one-half to one times the grid separation distance [5].

With the cell forward biased, one sees a change in the cell's photoresponse, the crack "signature," as one scans across the crack. Experimentally, one sometimes sees this manifested as a slope change or an amplitude change in the photoresponse scan. A slope change could be caused by carrier recombination at the crack or by shunting leakage currents [5]. Amplitude discontinuities can be expected if the crack is closer to one metallization finger than another [5]. A crack between a pair of metallization grids should not influence the photoresponse outside that region. Occasionally it does, and some areas of the cells delineated by cracks may exhibit a lowered scanning response everywhere. This could be due to differences in resistances between the cell output electrodes and the various semiconductor regions contacted.

A number of cells were inspected for cracks. All cracks which were previously located with the use of a microscope were readily found with the scanner. The cells were forward biased with values of current not markedly different from those that would exist within the cells with the cells exposed to their normal solar insolation. In some cells with smooth surfaces, for which visual inspection should work best, cracks were visually observed to begin at cell edges and appeared to end within a short distance. Laser scanning with the cells forward biased easily confirmed the location of all cracks so located visually, and equally important, the crack signatures indicated that the crack lengths were always greater than those visually observed. For some of these cases, crack signatures were observed across the entire cell. Other smooth-surface cells that had passed visual inspection as "crack free" were similarly scanned, and some of these also exhibited crack signatures. One practical implication of these results is that one may now determine when a cell has developed a crack wide enough to influence its operation. In the past, it has been difficult to say whether this occurred in array service, whether this occurred during array fabrication, or whether the cells for these arrays were received in this state from the manufacturer. This question can now be answered and should permit one to achieve enhanced array reliability.

Figure 10 shows scanning results obtained from a 100-mm (4-in.) diameter *n*-on-*p* single crystal silicon cell that was purchased commercially and found to have a crack. The results of scanning two small portions of the cell illustrate both the slope-change and amplitude-change predictions discussed above. The vertical lines are shadows of the metallization stripes which are spaced 2 mm (0.08 in.), center to center. The diagonal "troughs" in the lower right-hand corner of figure 10a and 10b are shadows of the wider metalli-

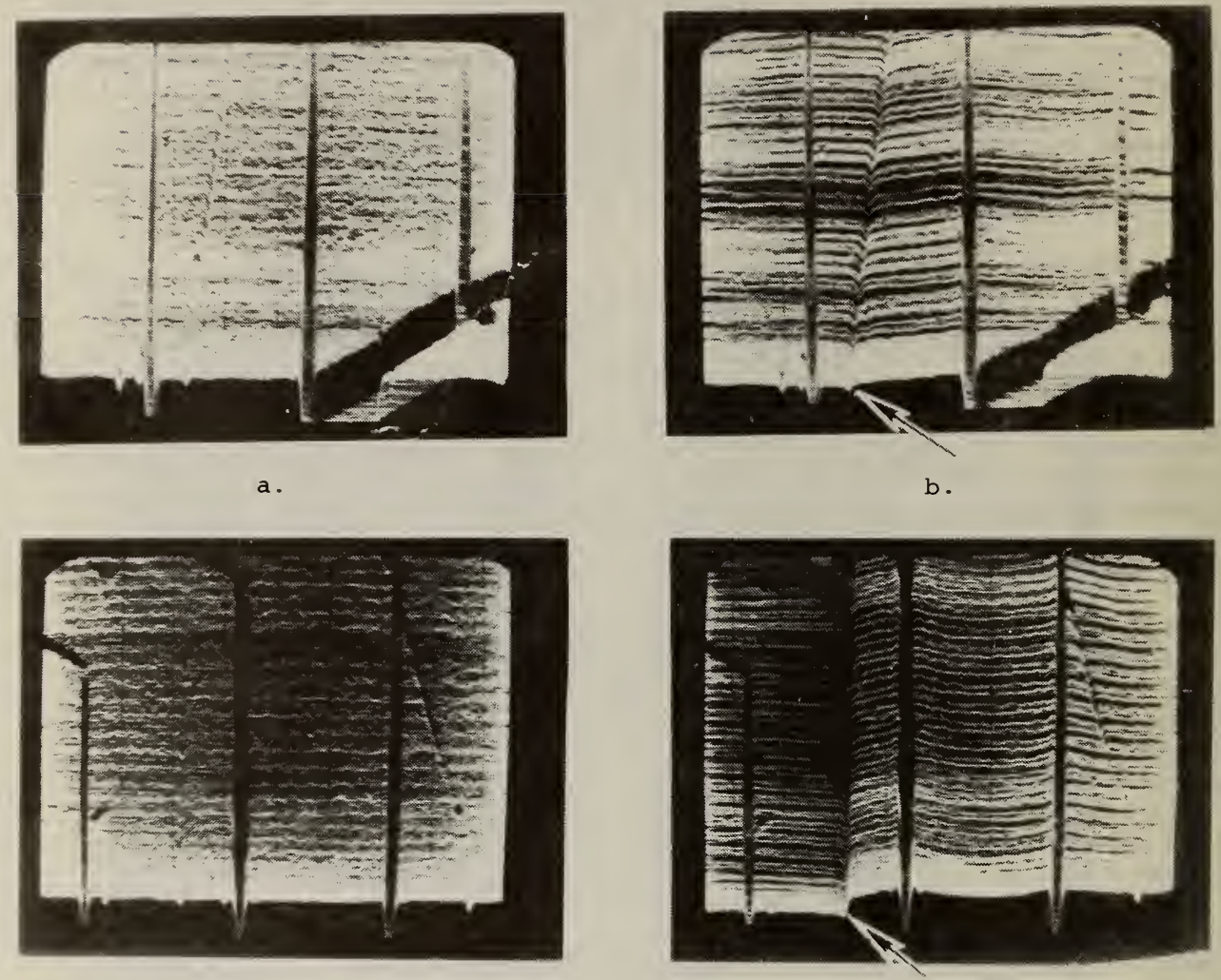

Figure 10. The results of scanning two small portions of a cracked 100-mm (4-in.) diameter silicon cell using the y-axis display mode. (a) Scanning photoresponse of the first portion with the cell unbiased. (b) Scanning photoresponse of the same portion as shown in (a) but with a cell bias of 0.9 A. (c) Scanning photoresponse of the second portion with the cell unbiased. (d) Scanning response of the same portion as shown in (c) but with a cell bias of 0.9 A. The cell crack location is indicated by arrows in (b) and (d).

zation buses which connect the metallization stripes to each other and to the top output electrode.

Figures 10a and 10c show the scanning responses of the two cell portions when a zero-bias current is applied, while figures 10b and 10d show the responses when a current of 0.9 A is supplied by an external current source. This current is about 29 percent of the current which the cell could produce were it crack free and exposed to one sun insolation. For this cell, it was possible to determine the crack location by optical inspection. The crack coincided with the scan response discontinuities appearing in figures 10b and 10d. In the display photographs, several surface features can be seen that are not cracks but show similar zero-bias scanning signatures. These features appear to be benign and may be due to scratches, dislocation lines, or the presence of unwanted material. One such feature, which is at an angle to the grids in figures 10c and 10d, was identified (with an optical microscope) as a thin film of the gridding metal. Since cell cracks (when they are wide enough to produce photoresponse perturbations without the cell being biased) and cell blemishes can yield the same zero-bias scanning signature, the harmless features could be mistakenly labeled as cracks and the cell rejected needlessly. Alternatively, a true crack might be mistaken as a benign cosmetic blemish. This set of photographs suggests that separation of these classes can be accomplished with forward-bias scanning.

4.1.2.4 Other Scanning Results

The following solar cells and cell prototypes have been laser scanned using the techniques described: GaAs concentrator cells, Cu_2S/CdS and Cu_2S/Cd[Zn]S cells, a thin-film polycrystalline silicon cell, EFG polycrystalline silicon cells, MIS single-crystal GaAs prototypes, silicon vertical junction and tandem junction cells, and both n-on-p and p-on-n junction flat-plate silicon cells. In addition to detecting metallization defects and crystal cracks described in the previous sections, the technique described has been used to:

1. Identify some portion of an MIS cell with significantly smaller photoresponse than the rest of the cell. This is felt to be due to "island formation," e.g., break-up of the thin, optically transparent metal film which may occur in these structures during storage or during service.

2. Provide information useful to the cell design physicist. For example, it was found for a manufacturer's run of polycrystalline silicon cells that the same cell areas which had a zero-bias 1.15-μm photoresponse about one-half of that for the rest also showed a decrease in the 0.633-μm photoresponse for forward-bias currents corresponding to irradiance values of about one sun. The first observation suggested that the areas in question had poor back contact reflectance, and the second indicated poor ohmic contacts. Combining these two observations permitted the underlying cell design and fabrication problem to be understood and corrected.

4.1.2.5 Further Applications of the Laser Scanner

Experience gained during the course of the observations reported above leads to the following suggestions for utilizing the solar cell scanning method:

1. Cell metallization-efficacy testing can be done under production line conditions by unskilled personnel. With the equipment set up for a particular cell type and using the intensity-modulation display mode, one only requires that the operator note if a "dark line" (shadow of the metallization stripe) runs through the center of a "dark region." No knowledge of devices or fabrication processes is required of the operator.

2. By dividing the scanning response under bias with the zero-bias response on a spatial point-by-point basis, the fabrication and service-related cell loss mechanisms should be even easier to perceive and measure. The eye can make comparisons of this sort to some extent, but it might be better to use a computer.

3. The scanning technique developed may be very useful for monitoring solar cell degradation processes. For example, it is quite possible that early changes in metallization efficacy for GaAs concentrator solar cells could be detected by the technique. This cell type, because of its severe service operating conditions of large diurnal variations in temperature, large cell current densities, and possible exposure to corrosive environments, might be expected to show significant changes over its lifetime.

4.2 Equipment for Light-Biasing Cells

The analytical results presented in figure 7 show that in order to reliably observe cell defects such as cracks and metallization discontinuities in flat-plate (nonconcentrator) cells, the illuminator for forward biasing the cells during scanning should have the capability of producing cell short-circuit current response equivalent to exposing the cell to an insolation of about 20 suns. Noise and modulation of the light by, e.g., an inadequately filtered lamp power supply, should be minimized; otherwise, the scanner signal-amplifiers will process this extraneous optical signal along with the cell response to the laser scanning spot and obscure the display information.

Various light sources were investigated. Those considered first were high-pressure xenon gas discharge lamps such as are used in solar simulators. One such lamp was set up in a test bench and powered by a filtered dc source. Monitoring the light output with a photodiode revealed spikes and noise bursts which at times exceeded ten percent of the average light output and which had frequency components measurable to about 35 MHz. A dual-trace oscilloscope simultaneously monitoring the light output and the lamp voltage showed that the extraneous light signal originated within the lamp; undoubtedly, this is associated with instabilities inherent in the plasma discharge. It was concluded that, while such sources may be "quiet" enough for use in solar simulators where one is concerned with the average value of the light, they are not suitable for use as a laser scanner bias source.

Quartz-halogen incandescent sources were next investigated. A new model quartz-halogen high-intensity illuminator designed to be used with the same model microscope as the one incorporated in the scanner was tried, but the results were disappointing; the short-circuit cell current for a small area (2- by 2-cm) (0.8- by 0.8-in.) cell was less than one-sun irradiance. An examination of the optical path between the lamp and the specimen stage showed

that although the illuminator was more than adequate for its intended usage, it was not designed for efficient utilization of the lamp's output, and the optics between the illuminator and the specimen constituted a high f-number system. It became apparent that an illuminator tailored to the project needs had to be designed.

An insolation source was successfully designed around a quartz-halogen high-intensity lamp by using four flexible fiber-optic light pipes to direct the light to the cell area being scanned. With this new source, irradiance levels of about 20 suns can be produced at the surface of cells measuring 1 cm by 1 cm. The optical system uses four groups of heat filters and condensing and focusing lenses arranged symmetrically around the long axis of the lamp. This arrangement captures most of the light available from the lamp.

An elusive source of modulation of light from the insolation source was located and eliminated. Vibration from the lamp cooling fan fastened to the bottom of the lamp and lens assembly housing was found to be the source of the undesired modulation. Any motion of the light-source components relative to one another can change the amount of light transmitted to the light pipe bundles and, hence, can change the light emerging from the bundles and incident on the cell specimen. The problem was solved by providing a separate support for the lamp housing and the cooling fan. This possible source of vibration should be kept in mind by anyone attempting to duplicate the light-bias equipment.

A photograph of the light source with the top cover removed is shown in figure 11. A small silicon solar cell, mounted inside the illuminator, powers an external meter to monitor the light from the lamp. This circuit permits one to set the lamp power easily. Because neither the uniformity nor the exact value of the cell illumination was found to be a critical parameter when the illuminator was used with the scanner to detect cell defects, this technique provides adequate control of the light output at the ends of the fiber-optic pipes. Figure 12 gives an overall view of the illuminator with fiber-optic light pipes. Figure 13 is a photograph of the scanner taken shortly after the illuminator was put in service. Figure 14 is a close-up view of the specimen stage; the cell being scanned is a 2- by 2-cm "space" cell. The clamp arrangement visible in figures 13 and 14 was an interim arrangement to allow the light-emitting ends of the fiber-optic pipes to be positioned relative to the cell. A more versatile arrangement is described in the following paragraph.

For a given cell, one may need to use a variety of scanner lenses to investigate various cell phenomena. The cell height relative to the scanner frame may change as one changes from one lens system to another. The position at the fiber-optic bundles must be adjustable to accommodate these changes in cell height and also to allow one to modify at will the pattern of bias light at the cell, as one changes from one cell to another having a different area. To satisfy these needs, a very versatile clamping system was constructed which permits each set of two fiber-optic bundles (one set on the left and one on the right) to be moved vertically and horizontally. Additionally, each of the four bundles can be individually oriented. This system can be seen in figure 15, although the light-biasing apparatus was not in use when the photograph was taken. This picture was made near the end of the report-

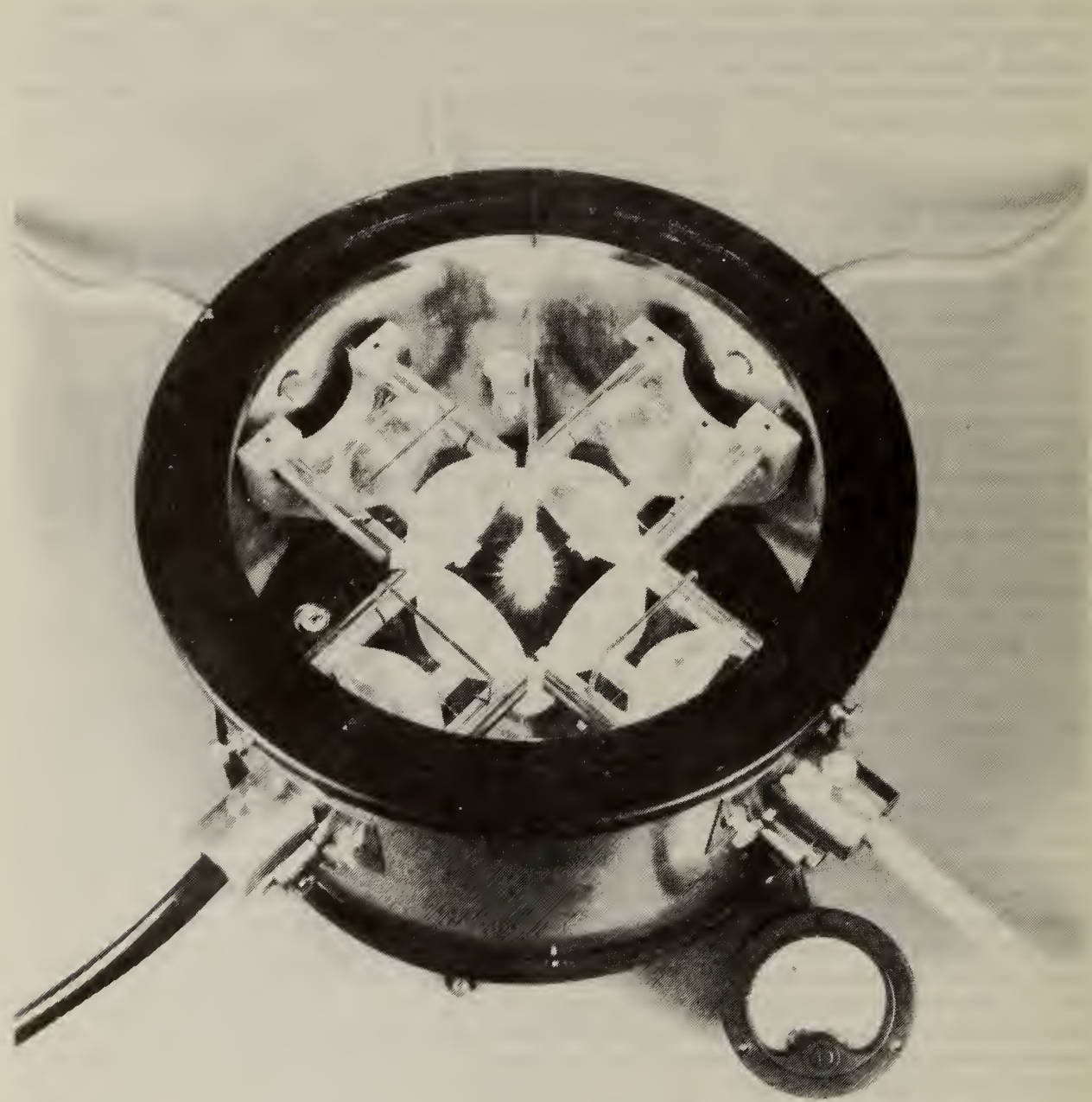

Figure 11. The high-intensity light source with the top cover removed.

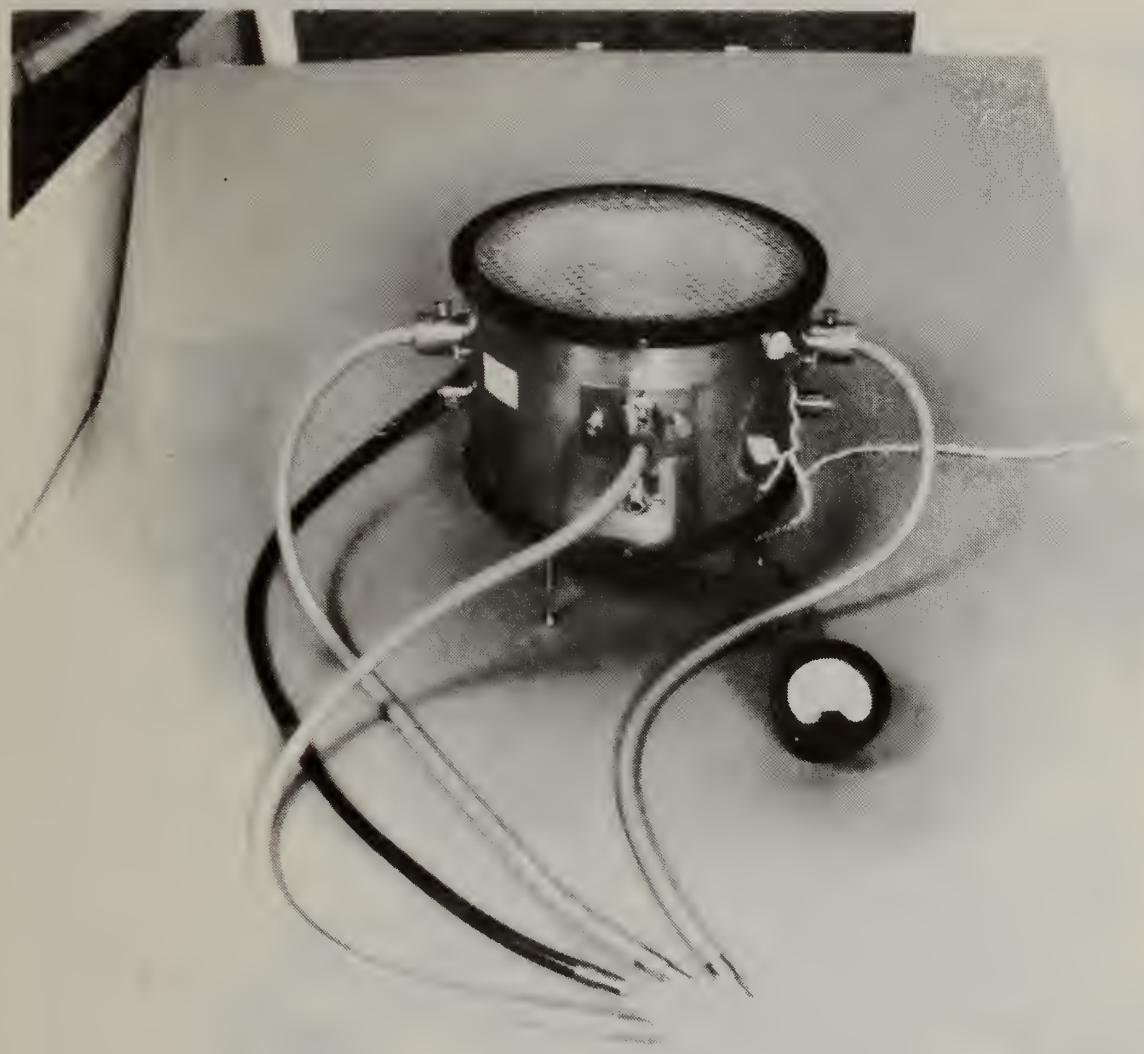

Figure 12. An overall view of the high-intensity light source including fiber-optic light pipes.

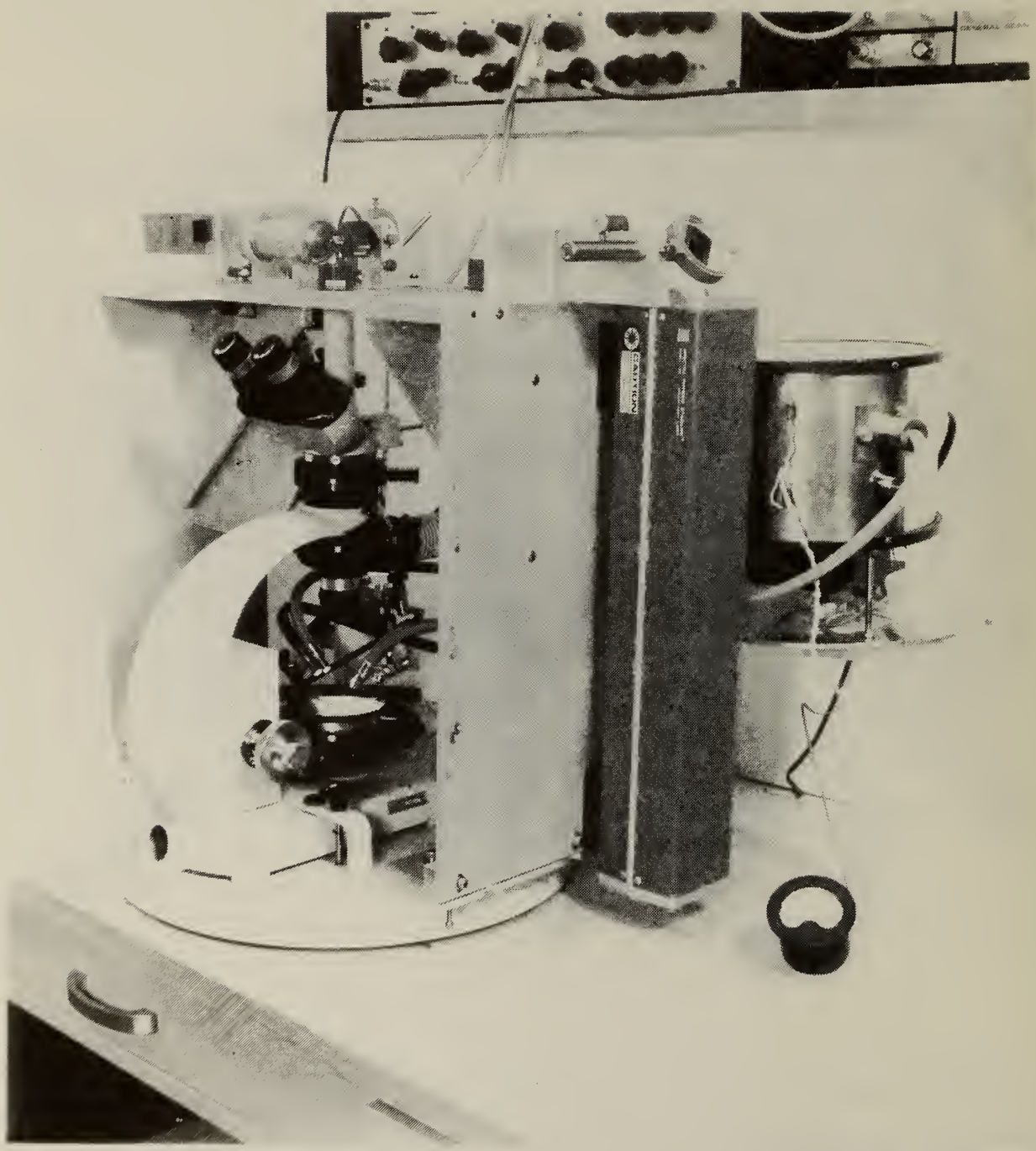

Figure 13. The illuminator being used during the laser scanning of a solar cell.

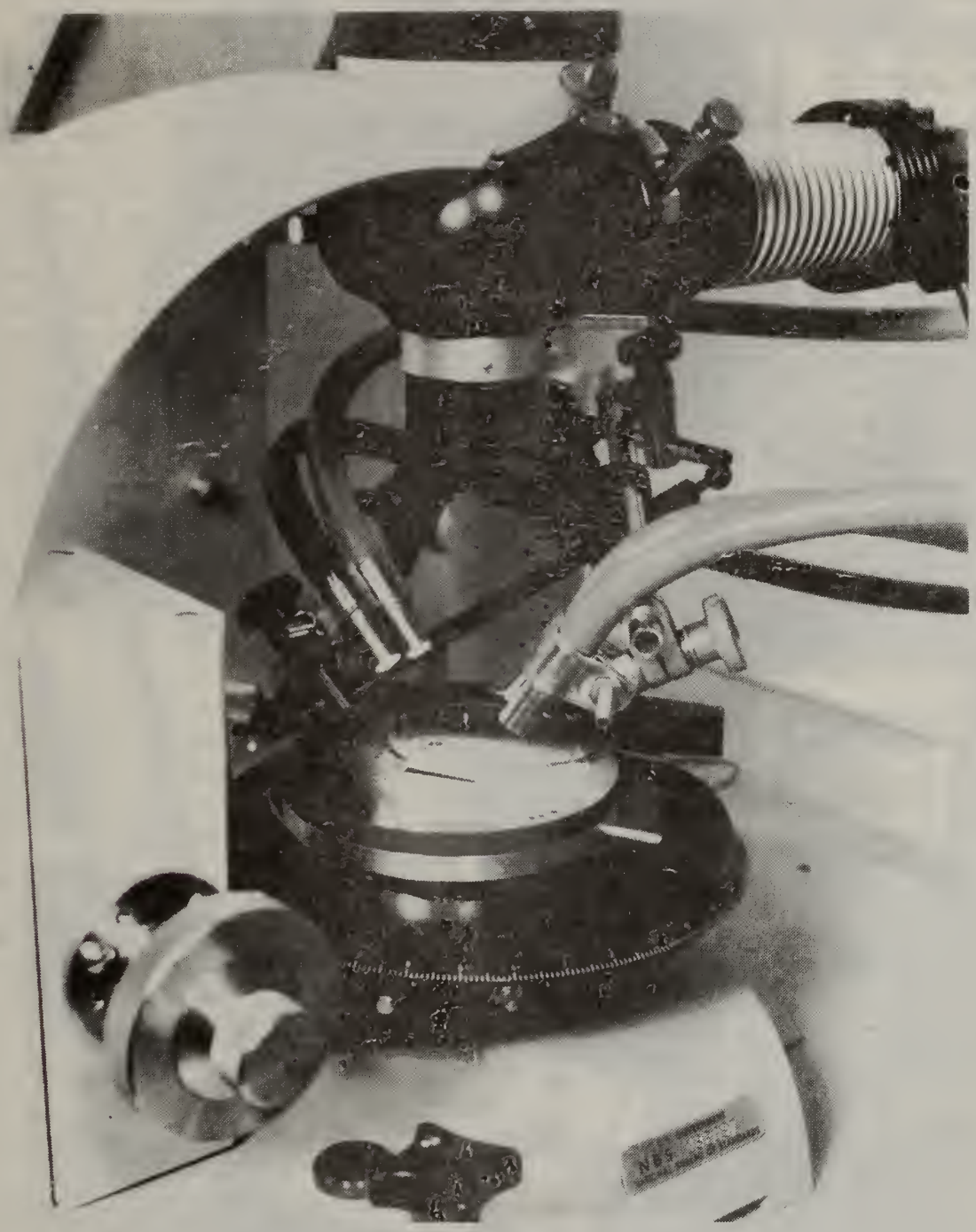

Figure 14. A close-up view showing the means used to adjust and clamp the light-emerging ends of the fiber-optic light pipes.

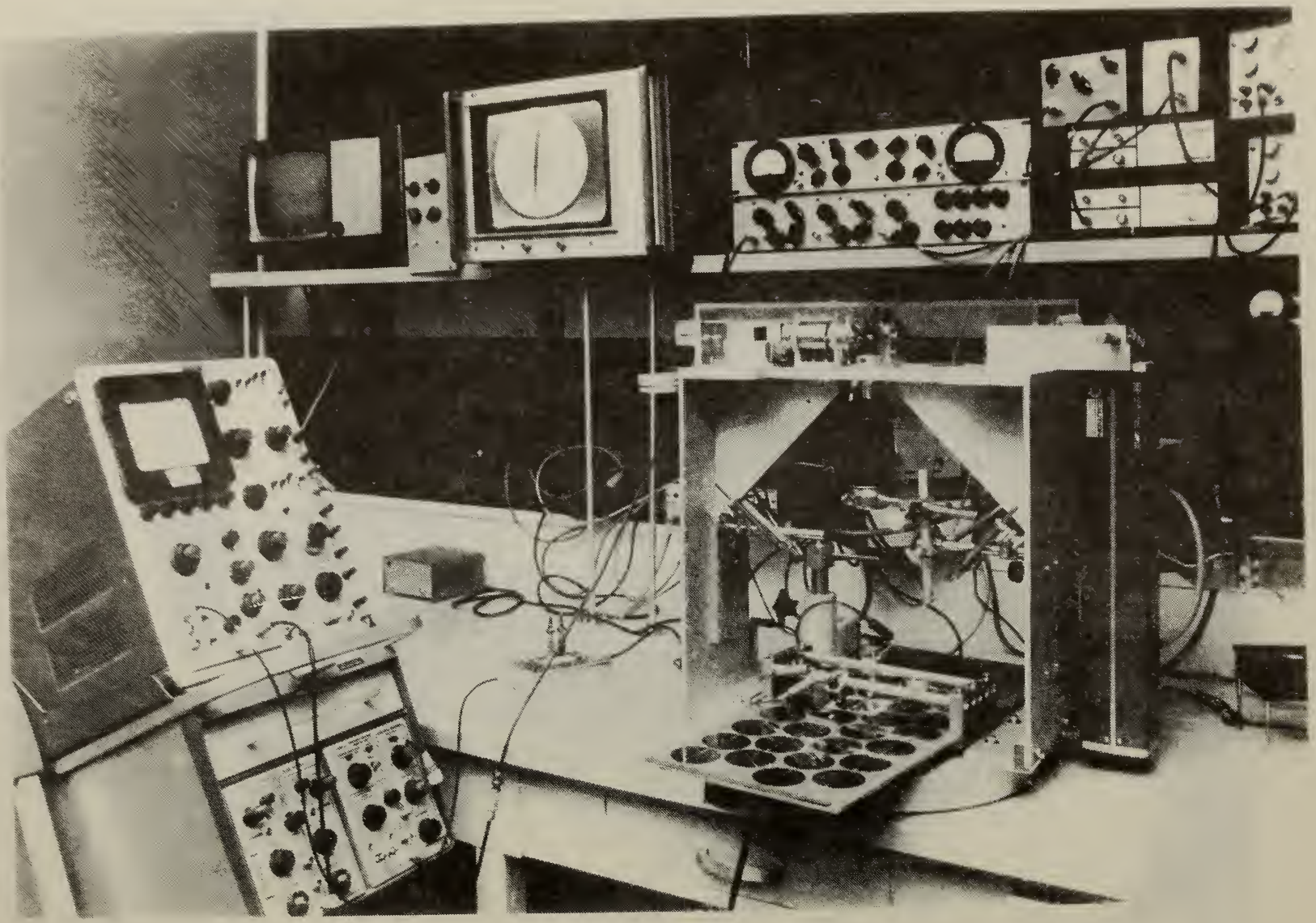

Figure 15. A photograph taken near the end of the reporting period of the laser scanner and some of the ancillary equipment described in this report. One of the 5.63-cm (2.25-in.) diameter cells in a 36-cell module is being scanned.

ing period, and it shows the microscope replaced by other optical elements; it also shows ancillary apparatus used and developed during the period. The other optical arrangements and the ancillary apparatus are discussed in sections 4.3 and 4.4, respectively.

4.3 Laser Flying-Spot Scanner Modifications

A series of modifications was made to the scanner so that the cell size that can be scanned at one setting of the equipment was increased. Before the solar cell program was begun, the scan excursion was limited to a square area about 3 mm on a side by the optical parts available for the particular microscope used for the scanner optics. This excursion was adequate for scanning integrated circuits, discrete diodes, and transistors to obtain useful information about the point-by-point spatial operation of these devices (Appendix A), but most solar cells are larger than 3 mm square and so could not be scanned without repositioning. By changing the objective lens system for the original microscope, the scan excursion was increased to 11.5 mm, and the working (objective lens to specimen) distance was also increased to permit the inclusion of the optical-bias fiber-optic pipes described in section 4.2. Additional increases in scan area and working distance were achieved by replacing the entire microscope optical system (with the exception of the microscope ocular lens) with a 35-mm single-lens-reflex camera lens having a focal length of 55 mm. The maximum scan excursion is now 100 mm (4 in.) with a spot size of about 25 μm. The resolution achieved with this spot size is adequate to resolve the finest metallization grids found on nonconcentrator solar cells.

Figure 15 shows the photoresponse of one of the 5.63-cm (2.25-in.) diameter cells in a 36-cell module scanned with 0.633-μm laser light. The picture was made with a time exposure of about 5 s to capture the entire display screen image of the cell photoresponse. A flash exposure was used to superimpose an image of the equipment on the film negative. The frame fixture for the 25- by 60-cm (10- by 24-in.) cell module was constructed with a clamp arrangement which can be slid along the long dimension of the module and locked at any location desired. Electrical contacts are carried on spring-loaded probes traveling on parallel rods at right angles to the long dimension of the frame and module. Connections to the desired cell are made by pressing the probes through the transparent plastic array cover to contact the cell output leads.

4.4 Ancillary Apparatus

4.4.1 Solar Cell Impedance-Matching Network and Preamplifier

The capacitance associated with the injection of minority carriers in forward-biased solar cells may severely limit the spot deflection scanning rates allowable, when one employs the method to pin-point cell defects described above. One way of solving this problem is to reduce the RC time-constant of the cell and its load. This reduction can be accomplished by coupling the cell to the scanner display electronics with a transformer input. By matching the low dynamic resistance of the cell to the display input resistance with a suitable transformer, one also maintains the cell's intrin-

sic signal-to-noise ratio, which would otherwise be degraded if one simply connected the cell to the high input impedance of the display electronics.

Because the cell is forward biased during scanning, one cannot connect the transformer directly across the cell, but a dc blocking capacitor must be placed in series with the transformer primary. The reactance of the capacitor must be small compared with the transformer input impedance at the lowest frequency component originating from the scanned cell.

Figure 16 is the schematic diagram of the complete coupling network. Two 56,000 μF, 30-V dc electrolytic capacitors, labeled C_1, C_2, are connected back-to-back yielding an effective value of 28,000 μF. This arrangement allows cell biases (relative to the cell "base") to be either positive (for *p*-on-*n* cells) or negative (for *n*-on-*p* cells) without danger of capacitor damage. As a rule, the impedance of electrolytic capacitors tends to rise with frequency. The purpose of C_3 is to provide a low impedance path at these higher frequencies. An 80-V dc low-loss capacitor having a value of 0.5 μF was found to be a suitable choice for C_3. The wire-wound noninductive resistor connecting the cell to the bias supply has a resistive of about 15 Ω. The impedance matching resistor across the transformer secondary has a resistance of 50 kΩ. A stable, adjustable, and well-filtered dc source serves as the bias supply. Other general-purpose laboratory power supplies have also been tried and found to be satisfactory.

A number of matching transformers, T_1, each having input impedances of the order of 1 Ω were tested. One test was to measure the frequency response of the transformer under impedance-matched conditions to simulate actual operation. To achieve impedance matching, a simple resistive network was inserted between the signal source and transformer to present a 1-Ω effective source impedance to the transformer primary. A 50-kΩ impedance matching resistor was connected across the transformer secondary. The criterion for this test which used to be transformer selection option was the separation of upper-to-lower cutoff frequencies. The larger the separation, the better the transformer. The other test, also performed under impedance-matched conditions, was of the response of the transformer to a simulated video signal. The response was tested by using square waves with a repetition frequency in the middle of the transformer's pass-band. The criterion for selection was that the transformer output waveform should be a good replica of the input waveform, that is, no significant overshoot, droop, or ringing should be observed. The transformer chosen as the most suitable for incorporation into the circuit had been designed to serve as a step-up transformer for coupling a phonograph cartridge to a preamplifier in a high-fidelty audio system. Compared with simply connecting a solar cell to the scanner display electronics, use of the transformer increased the signal about 35 dB and increased the signal-to-noise ratio 30 dB. The completed matching network, which has a flat frequency response from 5 Hz to 13 kHz (3 dB points), is housed in a 5.1- by 7.6- by 12.7-cm (2- by 3- by 5-in.) aluminum rectangular box.

The preamplifier is the plug-in signal amplifier of a general purpose oscilloscope, and it is powered by the oscilloscope. The amplifier has a front panel output jack which feeds the scanner display. The solar cell scanning response is also displayed on the oscilloscope screen for direct monitoring.

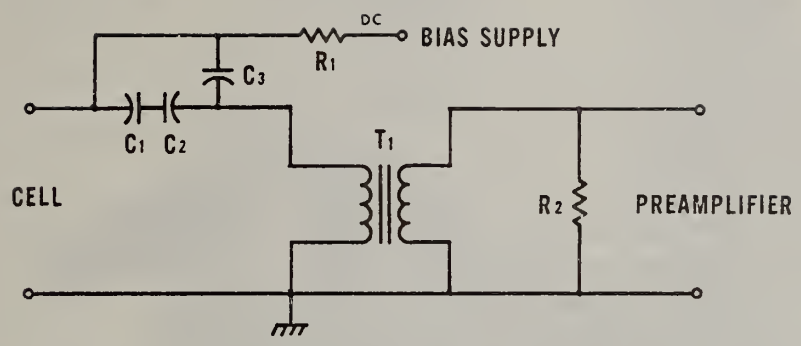

Figure 16. Schematic diagram of the solar cell coupling network. The criteria for the selection of the components and the component part values are stated in the text.

The plug-in amplifier has gain controls which permit one to maintain, by monitoring the oscilloscope presentation, the peak-to-peak signal level fed to the display screen electronics for bias-on, bias-off cell scanning measurements. This allows one, by glancing from one photograph of the display screen to another, to directly compare the effects of cell biasing. This system was used to produce most of the photograph sets shown in section 4.1.2. The noise characteristics of the plug-in amplifier were measured, and it was shown to produce only a few decibels of noise above the thermal level for frequencies within its pass-band when its input is connected to a 50-kΩ source impedance. The amplifier has separately adjustable low and high cut-off frequencies. By judicious selection of these frequencies, specimen noise outside of the cell scanning response spectrum is reduced to enhance the clarity of the display screen presentation.

4.4.2 Solar Cell Clamping and Rocking Stage

Most ICs and discrete transistors, studied before the present reporting period, were easy to mount for scanning since they usually came equipped with pins or wire leads which could be inserted in appropriate sockets clamped onto the microscope specimen stage. The plane of the scanned device could be easily adjusted by bending the device leads so that the light reflected from surface features such as metallization is directed toward the germanium photodiode used in the reflected-light circuit. However, neither the same holding arrangement nor the same method for aligning the reflected-light path is workable with the usual solar cell. The cell is usually flat, and if leads are an integral part of the cell, they are not normally adequate to hold the cell. To solve this problem, the clamping and rocking unit shown in figure 17 was designed and constructed to fit between the solar cell and the microscope x-y cross-slide stage; the x-y stage retains its original function of translating the scanned specimen perpendicular to the optical axis of the microscope. The upper part of the unit is a vacuum chuck having replaceable top plates to accommodate cells of various sizes. The rocking feature is controlled by the two micrometer heads that can be seen in the photograph. These permit precise rotation of the vacuum chuck around the x- and y-axes to direct the reflected light to the germanium photodiode. The chuck is spring loaded against the micrometer tips to maintain the settings of the micrometer heads.

4.5 Reference Structure Arrays

The results presented in section 4.1.2 show that the scanning techniques developed are quite effective in revealing cell defects. These results are qualitative, and one also needs to know the precision of the techniques developed. With this known, one would be able to measure defect magnitudes and cell parameters with a stated measurement accuracy to put the laser scanning technique on a firm quantitative basis.

To accomplish this, Reference Structure Arrays (RSAs), which are solar cells incorporating precisely known "defects" and known parameter variations and which are accompanied by ancillary test patterns, are to be fabricated and laser-scanned under planned bias and scanning conditions. The test patterns are designed to give independent measurements of the "defect" and parameter values. The laser scanning results are then to be compared with results ob-

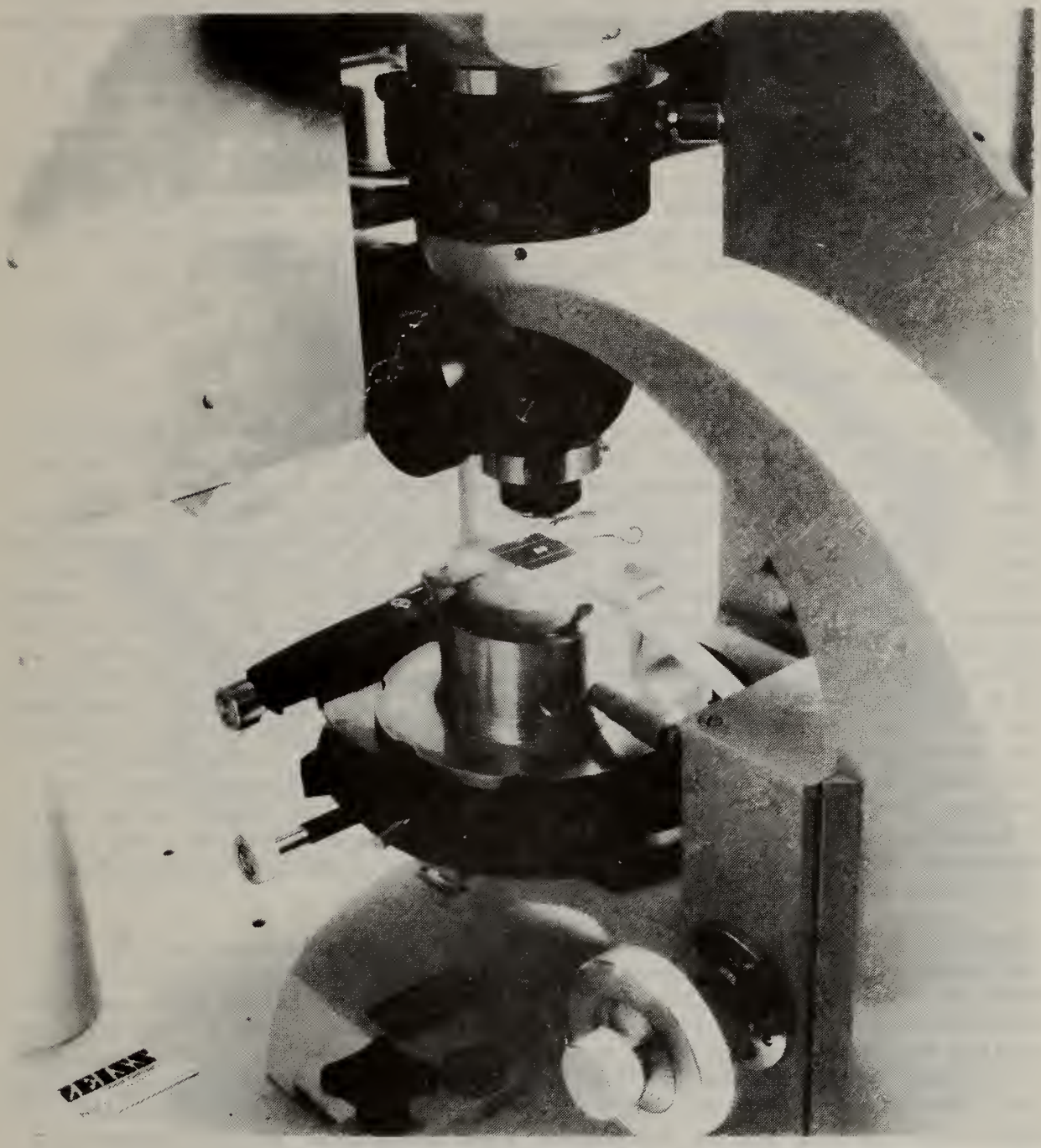

Figure 17. Solar cell clamping and rocking unit attached to the microscope cross-slide stage. Cell clamping is performed with a vacuum hold-down chuck magnetically held to the top plate of the rocking mechanism. Rocking (the orientation of the vertical axis) is controlled by micrometers. This photograph was made with the scanner in operation, and the scanning light raster is approximately in the middle of the cell.

tained by mathematical modeling such as described in section 4.6.3. During this reporting period, the design of the RSA was completed. The RSA consists of four solar cells, each surrounded by test patterns to give a mean value of, and the spatial variation in, cell and material properties and parameters including emitter and metallization sheet resistance, metal-to-emitter contact resistance, substrate resistivity, and carrier density in the base as a function of distance below the emitter-base junction. The first solar cell is "perfect," i.e., it contains no intentional defects; the second contains metallization-emitter open regions of various controlled sizes; the third has an emitter sheet resistance which varies periodically in a stripe pattern; and the fourth contains both opens and the periodically varying emitter sheet resistance. The RSAs will be constructed in single-crystal silicon, as only silicon technology offers the fabrication precision required.

4.6 Mathematical Analysis

4.6.1 Laser Scanning Using Microwave-Modulated Light

It is well known that the energy conversion efficiency of a cell may be severely reduced if the lateral resistance of the emitter is excessive, since all the photocurrent is constrained to flow laterally along the emitter. Thus, almost all junction solar cells employ gridding to reduce this resistance. Several gridding schemes may be employed. For example, the grids may be in the form of radial "spokes," or they may be in a cross-hatch pattern, but the most common pattern is a "finger" configuration. This is the configuration which is assumed in the analysis which follows. The purpose of this analysis is to determine the conditions under which the laser flying-spot scanner, using light modulated at high frequencies, can be used to determine in a nondamaging manner the sheet resistance of the emitter. With this known through measurements made on the cells themselves, one can attempt to control its value on later cells and optimize cell performance. After techniques have been developed for *in situ* emitter sheet resistance measurements, one can then work toward developing techniques for measuring variations in this resistance. The emitter sheet-resistance measurement technique which will be described uses only the contacts to the cell (the electrode terminals) which are always an integral part of the completed cell.

Figure 18 is the representation of a reverse-biased solar cell with grids in the finger configuration showing the passive cell elements. (If the cell were not reverse biased, the equivalent circuit would include additional passive elements representing the junction diffusion admittance.) The state of affairs depicted corresponds to an instant in time when the laser spot is approximately midway between the two grid stripes, shown by shading in the figure. The device equivalent circuit is that of a distributed resistance-capacitance network due to the emitter sheet resistance and the transition-region capacitance of the reverse-biased p-n junction. The net result of carrier photogeneration due to the laser spot is to place a current generator across the transition-region capacitance just below the light spot [6,7,8], as shown in the figure. If the light is modulated, then the equivalent current generator will have both ac and dc components. (There will always be a dc component, because it is not possible for light to have an average value of zero!) Intuitively, one would expect the ac voltage measured between the

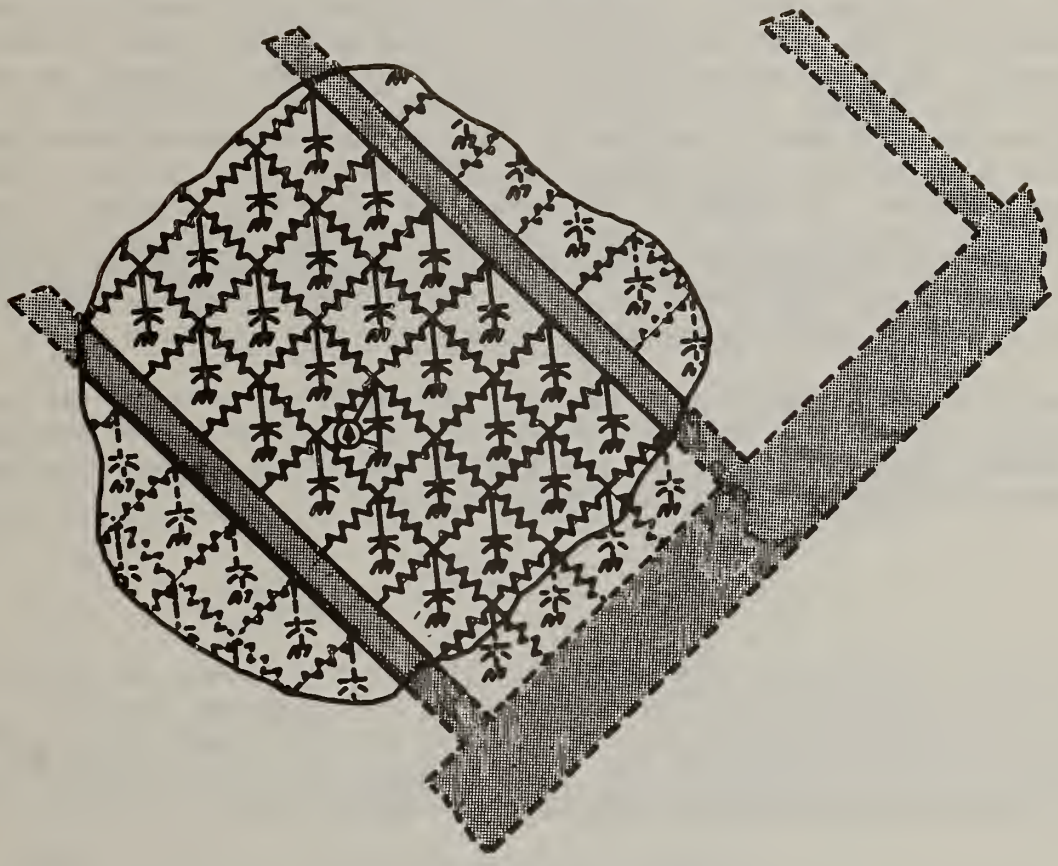

Figure 18. Representation of the two-dimensional parasitic resistance-capacitance nature of a reverse-biased solar cell.

top and bottom electrodes to vary with the location of the light spot, reaching a maximum just at the edge of a grid and a common trough-shaped minimum midway between a pair of grids. One would expect this because of the symmetry of the grid pattern and because of greater attenuation of the signal current by the two-dimensional resistance-capacitance network as the distance between the light spot and its nearest grid line is increased.

For the geometry shown, the analysis is simplified if a line of laser light parallel to the grids is used, rather than a spot, and the scanning is performed by moving the light line in a direction perpendicular to its length. The grids and this line of light are assumed to have the same length w. If the line is much longer than the separation of the grids, the problem can be treated as one-dimensional. Figure 4 is the equivalent electrical circuit of the portion of the solar cell between two grids separated, edge to edge, by a distance ℓ. Although scanning with a line of light will probably not be performed in the program, it is useful to analyze this one-dimensional case because the solution can be obtained in a closed-form expression which may be examined to anticipate the important results for the more realistic two-dimensional case. In figure 4, the scanning line is at a distance p from the edge of the left grid. It is clear that all such cell portions are equivalent. It is only necessary to analyze one. The impedance of the rest of the solar cell (as yet unspecified in value) may be lumped with the cell terminating impedance (also unspecified) to yield the load impedance Z_ℓ.

The equations relating the line current i(x) in the plane of the emitter, the voltage v(x) across the line, the capacitance per unit area c of the line, the emitter sheet resistance $\rho_\square$, the angular modulating frequency ω, and the coordinate distance x are easily derived and are

$$\frac{di(x)}{dx} = - j\omega cwv(x) \tag{7}$$

$$\frac{dv(x)}{dx} = - \frac{\rho_\square}{w} i(x) \tag{8}$$

where $j = (-1)^{1/2}$.

Differentiating eq (8) and substituting into eq (7),

$$\frac{d^2v(x)}{dx^2} - \beta^2 v(x) = 0 \tag{9}$$

where

$$\beta = (j\omega/\omega_0)^{1/2} , \tag{10}$$

and ω_0 is the angular frequency

$$\omega_0 \equiv (\rho_\square c)^{-1} . \tag{11}$$

The general solution of eq (9) is

$$v(x) = Ae^{\beta x} + Be^{-\beta x} . \tag{12}$$

The constants A and B are chosen to satisfy the boundary conditions. From eq (8), the line current is

$$i(x) = -\frac{w\beta}{\rho_\square}\left(Ae^{\beta x} - Be^{-\beta x}\right) . \tag{13}$$

Two sets of equations similar to eqs (12) and (13) are required: one to represent the line to the left of p, and the other for the line to the right of p. Designating the quantities to the left by the subscript I, and to the right by the subscript II, and with i_0 representing the magnitude of the current generator due to the modulated laser light, the two sets of equations are solved subject to the boundary conditions

$$i_{II}(p) - i_I(p) = i_0 \tag{14}$$

$$v_I(p) = v_{II}(p) \tag{15}$$

$$v_I(0) = v_{II}(\ell) = Z_\ell[i_{II}(\ell) - i_I(0)] . \tag{16}$$

The voltage across the load Z_ℓ, i.e., the output voltage v_{out} for the scanning light line at the arbitrary position $0 \leq p \leq \ell$ is

$$v_{out} = i_0 Z \frac{\{\sinh[\beta(\ell - p)] + \sinh(\beta p)\}}{\left\{\sinh(\beta\ell) + \frac{2w\beta Z_\ell}{\rho_\square}[\cosh(\beta\ell) - 1]\right\}} . \tag{17}$$

As the laser light line is swept from one grid stripe to another, v_{out} undergoes a maximum-minimum-maximum excursion having the ratio

$$\frac{v_{out}(min)}{v_{out}(max)} = \frac{v_{out/p = \ell/2}}{v_{out/p = 0}} = \text{sech}\ (\beta\ell/2) . \tag{18}$$

It is noteworthy that this ratio does not depend on the effective load impedance Z_ℓ. All the quantities in eq (18), with the exception of $\rho_\square$, are known, or can be found readily for the cell using nondamaging methods, and so selecting a value of $\rho_\square$ which brings eq (18) into agreement with the measured ratio $v_{out}(min)/v_{out}(max)$ yields the emitter sheet resistance.

4.6.2 Laser Scanning of Forward-Biased Cells.

For forward-biased cells scanned with a line of light, the pair of equations analogous to eqs (7) and (8) are

$$\frac{di(x)}{dx} = -w\sigma_p v(x) \tag{19}$$

$$\frac{dv(x)}{dx} = -\frac{\rho_\square}{w} i(x) , \tag{20}$$

where σ_p is the shunt conductance, due to forward-biasing, per unit area, and $\rho_\square$ is the emitter sheet resistance as before. By changing the definition of β used in section 4.6.1 to

$$\beta \equiv (\rho_{\square}\sigma_p)^{1/2} , \tag{21}$$

the resulting expressions for the output voltage, and the maximum-minimum-maximum voltage excursion are again given by eqs (17) and (18).

4.6.3 Mathematical Modeling Work Performed Under Subcontract with the University of Southern California*

4.6.3.1 Introduction

D. Sawyer and coworkers at NBS are scanning solar cells by a modulated light spot as a means to locate and identify cell faults by inspection of the cell output pattern. Their aim is the modeling of various faults and the computation of the resulting output patterns. Comparison of the computed patterns with observations will assist in identifying the faults in experimental cells.

The solar cell will be modeled by a two-dimensional distributed network of diodes connected by semiconductor sheets having sheet resistances ρ_T on top of the junction and ρ_S on the bottom. The corresponding bulk resistivities are Ω_T and Ω_S, respectively. An edge view of the model is shown in figure 19. The effect of light is to place a current source of total magnitude I_L across the diodes illuminated. A top view of the electrode configuration is shown in figure 20. The electrodes are of length W. Figure 21 shows an element of the distributed network of figure 19 and indicates the notation used in the analysis; $(x - x_1)$ is a delta function centered at $x = x_1$. The notation used here is consistent with that used in reference [9].

4.6.3.2 Basic Equations

The dark current per unit area J_D depends exponentially on the voltage across the junction:

$$J_D = J_o(e^{BV} - 1) . \tag{22}$$

The pre-exponential coefficient J_o is the reverse saturation current per unit area and $B = q/\alpha kT$ with α the diode quality factor.

Lateral diffusion currents are neglected so that the lateral sheet current densities are

$$\vec{J}_T = - \nabla V_T/\Omega_T \tag{23a}$$

and

$$\vec{J}_S = - \nabla V_S/\Omega_S , \tag{23b}$$

---

*This section of the report was prepared by K. Lehovec and A. Fedotowsky, Department of Electrical Engineering, University of Southern California, Los Angeles, CA 90007.

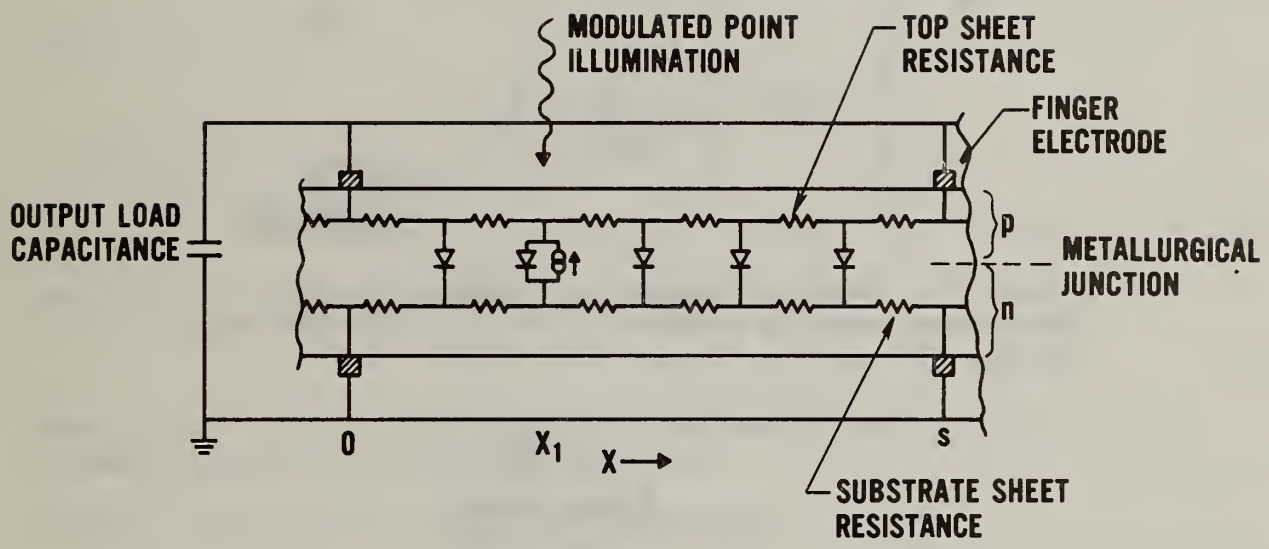

Figure 19. One-dimensional cross-section through the equivalent circuit of a solar cell portion illuminated by a modulated light beam at $x = x_1$. Output is ac-shorted by a large capacitive load.

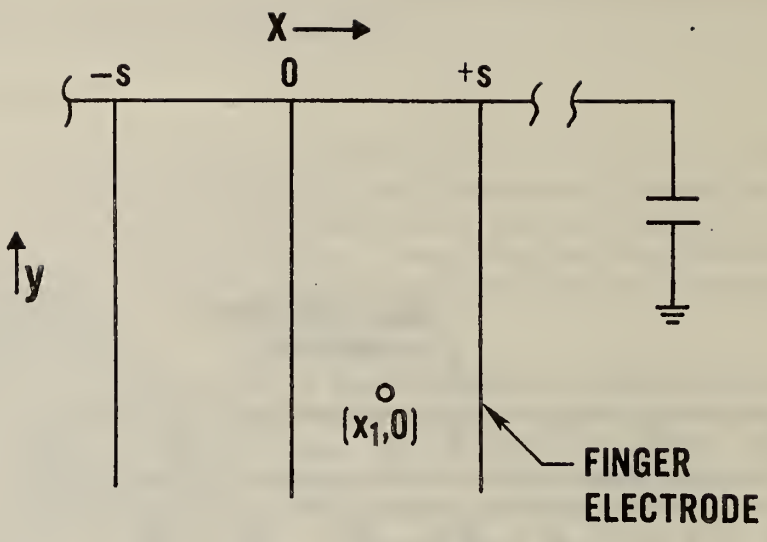

Figure 20. Sketch of a solar cell showing finger electrodes spaced by distance s and an illuminated spot at $(x_1, 0)$.

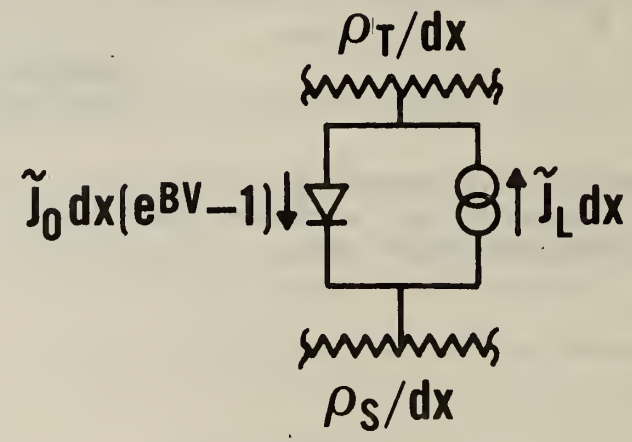

Figure 21. Element of the distributed network shown in figure 19 indicating the notation used in section 4.6.3.

where the subscripts refer to top and substrate (i.e., base) of the junction, respectively. Conservation of charge requires that

$$- \Omega_T/\rho_T \, \nabla\cdot\vec{J}_T + J_L - J_D = \partial Q_T/\partial t \tag{24a}$$

and

$$\Omega_S/\rho_S \, \nabla\cdot\vec{J}_S + J_L - J_D = - \partial Q_S/\partial t \tag{24b}$$

where Q_T and Q_S are the net charges per unit area above and below the metallurgical junction. Charge neutrality in any vertical section of the panel requires that $\partial Q_T/\partial t = - \partial Q_S/\partial t \equiv \partial Q/\partial t$. Substituting eqs (23a) and (23b) into eqs (24a) and (24b), respectively,

$$\nabla^2 V_T = - \rho_T [J_L - J_D - \partial Q/\partial t] \tag{25a}$$

and

$$\nabla^2 V_S = \rho_S [J_L - J_D - \partial Q/\partial t] \, , \tag{25b}$$

so that

$$\nabla^2 V \equiv \nabla^2 (V_T - V_S) = - (\rho_T + \rho_S) \cdot [J_L - J_D - \partial Q/\partial t] \, . \tag{26}$$

Now $\partial Q/\partial t \equiv \partial Q/\partial V \cdot \partial V/\partial t \equiv C \partial V/\partial t$, so that

$$\nabla^2 V = - \rho [J_L - J_D - C \partial V/\partial t] \tag{27}$$

with $\rho \equiv \rho_T + \rho_S$ the sum of the sheet resistances and $C = \partial Q/\partial V$ the incremental diode capacitance per unit area.

4.6.3.3 Low Intensity, Modulated Illumination

Next, consider the case of a generation current comprising dc and ac components:

$$J_L = \bar{J}_L + \tilde{J}_L \, . \tag{28}$$

There will then be both dc and ac voltage components:

$$V = \bar{V} + \tilde{V} \tag{29}$$

and eq (27) separates for small ac signals ($B\tilde{V} << 1$) into the relations

$$\nabla^2 \bar{V} = - \rho [\bar{J}_L - \bar{J}_D] \tag{30}$$

and

$$\nabla^2 \tilde{V} = - \rho [\tilde{J}_L - Y\tilde{V}] \, , \tag{31}$$

where

$$Y = G_D + j\omega C \tag{32}$$

is the diode admittance per unit area and $G_D = B(J_D + J_o)$ is the incremental diode conductance per unit area.

In the unilluminated region

$$\nabla^2 \tilde{V} = \tilde{V} Y \rho \ . \tag{33}$$

Since $Z = Z(V)$, there will be in general a positional dependence of ρ/Z. Equation (33) defines a position-dependent complex characteristic length. For scanning in the x-direction with a line of light oriented parallel with the electrodes, $\tilde{V}$ will vary only along the x-direction and the characteristic length may be designated x_o. It is convenient to work with the inverse of x_o. The inverse has both a real and an imaginary component, and these may be designated $(x_o')^{-1}$ and $(x_o'')^{-1}$, respectively,

$$x_o^{-1} = (x_o')^{-1} + j(x_o'')^{-1} = (Y\rho)^{1/2} \ . \tag{34}$$

The real part of this length provides an attenuation of V(x), while the imaginary part provides an oscillatory component. The characteristic decay length is

$$x_o' = \sqrt{1/\rho |\, Y \,|}\ /\cos(\phi/2) \tag{35}$$

and

$$x_o'' = \sqrt{1/\rho |\, Y \,|}\ /\sin(\phi/2) \ . \tag{36}$$

The wavelength of the oscillating component is

$$\lambda = 2\pi x_o'' = 2\pi\sqrt{1/\rho |\, Y \,|}\ /\sin(\phi/2) \ , \tag{37}$$

where

$$\phi = tg^{-1}\ (\omega C R_D) \tag{38}$$

and

$$|\, Y \,| = (R_D^{-2} + \omega^2 C^2)^{1/2} \ . \tag{39}$$

4.6.3.4 Fault-Free Cells Having Uniform Attenuation Lengths

These considerations are applied to the special case of a fault-free cell operated under the conditions that x_o defined in eq (34) is independent of position. This can be realized by using a cell without external bias and without background illumination, and by modulating the scanning light beam at a sufficiently high frequency that x_o has the desired value of about the finger electrode spacing s.

While the solution for line illumination of the perfect cell has previously been derived by D. Sawyer [10], its derivation here is still of interest as a

starting point for modeling of faulty cells, completed subsequent to the present reporting period.

4.6.3.5 Fault-Free Cells Illuminated by a Line-Shaped Light Beam

This line shape is of interest since it leads to simple analytical solutions. In case of only one pair of electrodes (at x = 0) of length w, one electrode contacting the top semiconductor sheet and the other contacting the bottom semiconductor sheet, the small-signal photovoltage for a short-circuit load is

$$\tilde{V}(x) = \tilde{I}_L x_0 \rho / w \begin{cases} e^{-x_1/x_0} \sinh(x/x_0) & \text{for } x \leq x_1 \\ e^{-x/x_0} \sinh(x_1/x_0) & \text{for } x \geq x_1 \end{cases} . \tag{40}$$

The photocurrent crossing unit length of a line parallel to the finger electrode and located at $0 \leq x \leq x_1$ is

$$\tilde{J} = \tilde{J}_L \exp(-x_1/x_0) \cosh x/x_0 . \tag{41}$$

The short-circuit output current is

$$\tilde{I}_{SC} = \tilde{I}_L \exp(-x_1/x_0) . \tag{42}$$

The quantities x_0' and x_0'' can be obtained from the magnitude

$$|\tilde{I}_{SC}| = |\tilde{I}_L| \exp(-x_1/x_0') \tag{43}$$

and phase

$$\text{Arg}(\tilde{I}_{SC}/\tilde{I}_L) = -x_1/x_0'' \tag{44}$$

of the short-circuit output current. The limit for $\tilde{I}_{SC}$ for $x_1 \to 0$ is $\tilde{I}_L$. From these data, R_D/ρ and CR_D can be derived. Thus, knowing the dc diode conductance per unit area, $1/R_D$, C and ρ can be determined.

The potential $\tilde{V}(x)$ in eq (40) has been composed of two exponential terms to satisfy the boundary conditions $\tilde{V}(x) = 0$ at the electrode x = 0. If a second finger electrode is considered at $x = s > x_1$, the boundary conditions $\tilde{V}(x) = 0$ at x = 0 and x = s may be satisfied by adding an infinite series of potentials from line source images with respect to these electrodes. This is a well-known procedure in electrostatic and optical problems. The result is

$$\tilde{V}(x) = \frac{\tilde{J}_L \rho x_0}{\sinh(s/x_0)} \begin{cases} \sinh(x/x_0)\sinh[(s-x_1)/x_0] & \text{for } 0 \leq x \leq x_1 \\ \sinh[(s-x)/x_0] \sinh(x_1/x_0) & \text{for } x_1 \leq x \leq s \end{cases} , \tag{45}$$

and

$$\tilde{I}_{SC} = \tilde{I}_L\{[\sinh[(s-x_1)/x_0] + \sinh(x_1/x_0)]\ /\sinh(s/x_0)\} \qquad (46)$$

where the first term in brackets results from the current collected by the finger electrode at x = s, and the second term results from the current collected by the finger electrode at x = 0.

4.6.3.6 Fault-Free Cells Illuminated by a Point of Light

The illumination of the point x_1, 0 induces the current source I_L at x_1, 0 in the equivalent circuit of figure 19. The resulting potential in the case of the presence of only one set of finger electrodes located at x = 0, i.e., assuming that $s - x_1 >> x_0$, is

$$\tilde{V}(x,y) = (\tilde{I}_L\rho/2\pi)[K_o(r^*(x_1)) - k_o(r^*(-x_1))] \qquad (47)$$

where

$$r^*(x_1) = [(x - x_1)^2 + y^2]^{1/2}/x_0 \qquad (48)$$

and K_o is a modified Bessel function of the second kind. The second term in the bracket of eq (47) results from the mirror image of the current source with respect to the finger electrode. The short-circuit current collected by the finger electrode is

$$\tilde{I}_{SC} = \rho^{-1}\int_{-\infty}^{+\infty} \partial\tilde{V}/\partial x)\Big|_{x=0} dy = (\tilde{I}_L x_1/\pi x_0)\int_{-\infty}^{+\infty} \frac{K_1(\sqrt{x_1^2 + y^2}/x_o)}{\sqrt{x_1^2 + y^2}}\, dy\ , \qquad (49)$$

assuming infinite finger electrode length. The integral is a simple case of the general Sonine-Gegenbauer Type [11]:

$$\tilde{I}_{SC} = \tilde{I}_L \exp(-x_1/x_0)\ . \qquad (50)$$

Note that the current for the point illumination is identical to the current, eq (42), for the line illumination. This result illustrates the equivalence theorem (to be proven generally in the next report) of current generated by point and line illumination. This equivalence theorem also applies to the case of two finger electrodes so that eq (45) derived for line illumination applies also to point illumination.

4.6.3.7 Output of Faulty Cells Having Noncontacting Electrode Sections

The general solution to the potential problem of a point current source located at $\vec{r}_1 \equiv (x_1, y_1)$ surrounded by an arbitrarily shaped ac grounded electrode contour Γ is

$$\tilde{V}(\vec{r}) = G(\vec{r}_1, r) - \int_\Gamma \tilde{J}(\vec{r}')G(|\vec{r} - \vec{r}'|\, d\vec{r}' \qquad (51)$$

where $G(\vec{r}_1, \vec{r}) = G(|\vec{r} - \vec{r}_1|)$ is the potential at $\vec{r}$ due to point source located at $\vec{r}_1$, and $\mathcal{J}(\vec{r}')$ is the current density entering the electrodes. This current density satisfies the integral equation

$$G(\vec{r}_1, \vec{r}') = \int_\Gamma \mathcal{J}(\vec{r}')G(|\vec{r} - \vec{r}'|)d\vec{r}' \tag{52}$$

thus assuring that $\tilde{V}(\vec{r}') = 0$. The effect of a poor electrode contact is taken into account by excluding the noncontacting electrode section from the contour. The poor-contact problem is mathematically related to a diffraction optical aperture problem.

5. WORKSHOPS

5.1 Stabilility of (Thin Film) Solar Cells and Materials

A workshop on the Stability of (Thin Film) Solar Cells and Materials was conducted at the National Bureau of Standards on May 1 to 3, 1978, as part of the Department of Energy's National Photovoltaic Program. The workshop program as issued to the attendees is included as Appendix B. The workshop addressed many of the problems and obstacles to achieving stability and long life of terrestrial, solar cell devices using current and projected technology. The following three groups of exploratory solar cell materials and concepts were considered: (1) [CdZn]S/Cu_2S, CdS/Cu-Ternaries, CdS/InP, and amorphous Si, (2) polycrystalline, MIS, and conducting oxide Si, and (3) polycrystalline and AMOS GaAs.

Researchers in the field reviewed modes and mechanisms for failure and degradation of these systems and the status of present reliability testing. Speakers from related device technologies discussed measurement and test approaches that they have used to achieve high device reliability. Two talks of particular interest described a technique for detecting changes in the physics of failure with increasing severity of a stress test to establish the maximum possible acceleration factor for a given failure and a technique for uncoupling different failure mechanisms from an analysis of failure rate data.

Discussions in the working groups of the workshop led to the identification of a number of needs that require attention before meaningful headway can be made in the achievement and quantification of stability and long life for solar cells developed using forefront materials and device technologies. Among the conclusions reached by the 102 scientists and engineers who attended the workshop was that more research needs to be conducted in this advanced technology. They identified the need to study the chemical, mechanical, and physical compatibility of the various materials used in these solar cell devices and their influence on device characteristics. Also expressed was the need for the development of performance and measurement standards for use in characterizing these devices. Finally, the need for adequate device manufacturing process controls and adequately described test procedures and data was underscored as a prerequisite for meaningful headway in the quantification of solar cell stability and long life. The proceedings of the workshop have been issued as NBS Special Publication 400-58.

5.2 Photovoltaic Material and Device Measurements

The Electron Devices Division of NBS and DOE/SERI began plans for a workshop on photovoltaic material and device measurements to be held in the Washington, DC, area in the spring of 1979. The purpose of the workshop is to accelerate the development of thin film solar cells by improving the versatility and reliability of material and device measurement techniques. Attendees at the DOE Annual Review Meeting for the Advanced Materials R&D Branch, Vail, Colorado, October 24 to 26, 1978 were given a questionnaire soliciting their thin film material and device measurement interests and perceived needs, and the workshop structure was conceived accordingly. The preliminary plans are included as Appendix C.

6. CONSULTATION AND LIAISON ACTIVITIES

A proposal for a novel photovoltaic converter was reviewed by D. E. Sawyer for DOE Headquarters.

D. E. Sawyer assisted in evaluating replies to DOE's RFP in Photovoltaic Mechanisms in Polycrystalline Thin Film Solar Cells, DOE Headquarters, July 24 to 27, 1978.

At the suggestion of the SERI Photovoltaic Program Office, D. E. Sawyer attended the December 18th Photovoltaic Session of the Workshop on Reliability of Materials for Solar Energy at Denver, Colorado, and participated in the session discussions. This workshop was organized by the Materials Branch of SERI's Research Division.

Nine solar cell invention submissions were given first-level review by D. E. Sawyer for the NBS Office of Energy-Related Inventions.

7. REFERENCES

1. Sawyer, D. E., A Technique for Using An Optical Scanner to Reveal Solar Cell Defects, *Proc. 13th IEEE Photovoltaic Specialists Conf.*, Washington, D.C., June 5-8, 1978, pp. 1249-1250 (1978).

2. Sawyer, D. E., Kessler, H. K., and Schafft, H. A., Solar Cell Measurement Technique Development and Other Services, *Proc. DoE Annual Review for Advanced Materials R&D Branch*, Vail, Colorado, October 24-26, 1978, pp. 41-50 (January 1979).

3. Hovel, H. J., Solar Cells, *Semiconductors and Semimetals*, R. K. Willardson and A. C. Beers, Eds., Vol. 11, p. 47 (Academic Press, New York, 1975).

4. Ross, R. G., private communication.

5. Lehovec, K., private communication. Preliminary results obtained under subcontract during present reporting period.

6. Gardner, W. W., Depletion-Layer Photoeffects in Semiconductors, *Phys. Rev.* 116, 84-87 (1959).

7. Anderson, L. K., Detection of Microwave Modulated Light, 1964 Int. Solid-State Circuits Conference Digest of Technical Papers, pp. 60-61.

8. Sawyer, D. E., A Study on p-n Junction Photodetectors Utilizing Internal Parametric Amplification, Sperry Rand Research Report SRRC-PR-65-34, issued April 1965, Final Report of Work Performed 1 April 1964 - 31 March 1965. Prepared for the Department of the Navy, Bureau of Naval Weapons, Research Division (RRRE-3), Washington, DC. Contract No. N600 (19) 61770.

9. Lehovec, K., and Fedotowsky, A., Degradation of Solar Cell Efficiency by Sheet Resistance, *Solar Energy* 21, 81-86 (1978).

10. Sawyer, D. E., Kessler, H. K., and Schafft, H. A., Measurement Techniques for Solar Cells, Quarterly Report, January 1 to March 31, 1978, NBSIR 78-1513 (September 1978).

11. Petian, G., La Théorie des Functions de Bessel, Centre National de la Recherche Scientifique, p. 210 (Paris, 1955).

APPENDIX A

Laser Scanning of Active Integrated Circuits and Discrete Semiconductor Devices*

D. E. Sawyer, D. W. Berning, and D. C. Lewis**

Institute for Applied Technology
National Bureau of Standards
Washington, D.C.

The device laser scanning work conducted in the Electronic Technology Division of the National Bureau of Standards (NBS) is described. The scanner constructed at NBS is sketched briefly; this is followed by illustrations demonstrating its usefulness for determining on a point-by-point basis the inner workings of active semiconductor devices. The scanner is non-damaging to all devices tried and it has been used to map d.c. and high-frequency gain variations in transistors, reveal areas of the device operating in a nonlinear manner, electronically map temperatures within devices, determine internal logic states in IC's and selectively change these states at will. It has also been used to perform hitherto impossible measurements on flip-chip bonded devices, that is, seeing the circuit electrical operation and the metallization pattern through the back side of the chip. Applications to other strucures and devices including solar cells are suggesed.

THE EFFECT OF DIRECTING LIGHT of energy somewhat greater than that of the band gap on a semiconductor is to create electron-hole pairs within the material which can be collected as a photocurrent. If the light is focused to a spot and moved over exposed semiconductor portions of a device, it is possible to learn a great deal about the internal operation of the device by interpreting the photoresponse. The interpretation is facilitated if the photoresponse is presented on the screen of a cathode ray tube whose electron beam is deflected in synchronism with the moving light spot since a "picture" of the photoresponse of the device is presented. Interpretation of the display can yield, on a point-by-point basis, information about the device which can be used to determine internal characteristics. This probing technique has applications in device testing, device design, and reliability. Provided that the photon energy of the light is less than a few times the band gap energy of the semiconductor one would not expect either short or long term device degradation to occur due to the light (provided of course that the optical power density at the specimen is not excessive). No device damage due to the flying-spot scanner has been observed.

Scanner Description

The scanner to be described here is based on previous work[1,2,3] and several innovations. A schematic outline of the scanner is shown in Fig. 1; a photograph of the apparatus is shown in Fig. 2.

Light for the laser scanner is provided by either of two low power He-Ne cw lasers. The wavelength of one laser is 1.15 μm; the wavelength of the second laser is 0.633 μm.

Mirrors M_1 and M_2 are used to fold the output from the 1.15-μm beam so that the scanner can be made more compact and rugged; mirror M_4 is used for the same purpose with the 0.633-μm beam. Mirror M_3 is used to select which laser output is to be used with the scanner; it can be used to block the 1.15-μm beam and simultaneously insert the 0.633-μm beam into the scanner, or it can be used to deflect the 0.633-μm beam out of the optical circuit of the scanner.

The analyzer shown at the output of the 0.633-μm laser in Fig. 1 is used to control the intensity of the radiation delivered to the device under test. Since the output of the laser is plane polarized, rotation of the analyzer can vary the transmissivity from 0 to 1. There is no intensity control on the 1.15-μm laser.

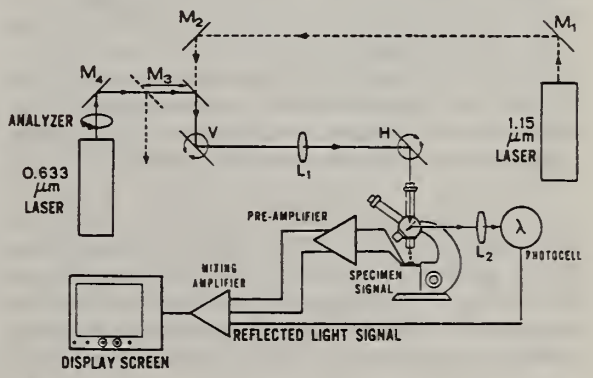

Fig. 1—The light and signal paths of the dual laser scanner.

*This work was conducted as part of the National Bureau of Standards program on Semiconductor Measurement Technology with principal funding from the Defense Advanced Research Projects Agency through ARPA Order 2397.

**Present address: Office of Naval Research, Washington, DC 22217.

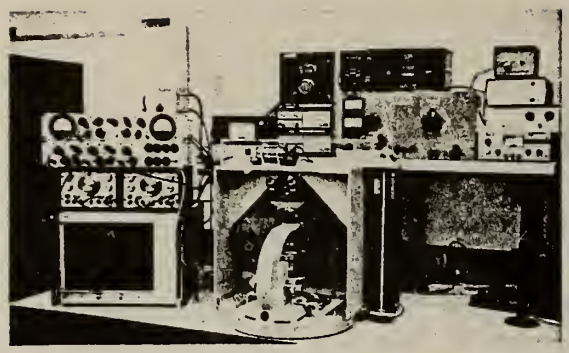

Fig. 2—Photograph of the laser scanner.

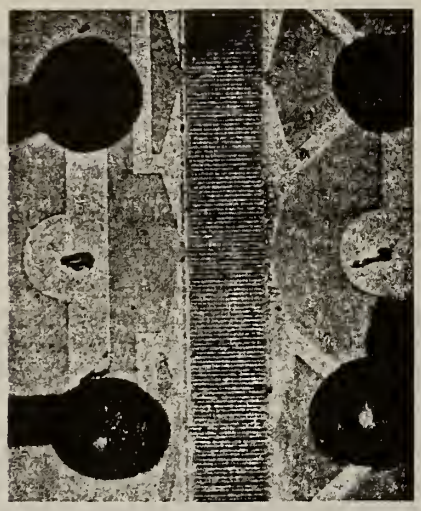

Fig. 3—Optical photograph of the surface topology for a microwave transistor consisting of four cells.

Mirrors V and H are electrically driven to provide orthogonal deflections of the light beam. Light from mirror H passes through a microscope and is focused to a spot on the device to be examined. The same electrical signals that drive mirrors V and H also deflect a spot on a cathode ray display screen in synchronism with the laser scan. The display screen is on the lower left of Fig. 1. The lens L_1 between the vertical and horizontal deflection mirrors refocuses the vertical deflection from V onto the horizontal mirror, H. The beam diverges from the horizontal deflection mirror, H, to form the scanning raster. The scan raster typically covers the same field of view that can be seen with the eye when the microscope is used in its customary manner. Light reflected from the specimen is used to identify the portion of the specimen being scanned. The reflected-light circuit uses a half-silvered mirror in the microscope which is an integral part of the microscope's vertical illuminator, a lens L_2, and a photocell. Laser radiation reflected from any point on the specimen is directed by the half-silvered mirror onto the lens and is focused to a fixed point on the photocell. The photocell signal modulates the display screen to present a picture of the device surface topography. Used this way, one could call the apparatus a "flying-spot microscope." The primary purpose of the reflected-light circuit is to permit correlation of the device response with surface features such as metallization areas. This is accomplished simply by mixing together the signals from the scanned specimen and the photocell. Alternatively, a color display screen has been used with the photocell signal fed into one color channel and the electrical signal(s) from the scanned specimen into the other(s). A recent publication[4] describes in detail the construction and operation of the entire scanner.

Two lasers are used for a greater measurement flexibility. Visible or near-infrared radiation incident on silicon creates electron-hole pairs with a generation rate which exponentially trails off with distance into the material. The penetration depends on the wavelength of the incident radiation. The visible light from the 0.633-μm laser has a characteristic penetration depth of about 3 μm in silicon.[5] Because most modern silicon devices have their active regions within a few micrometers of the surface, the 0.633-μm laser is quite effective in exciting active regions of silicon operating devices. The intensity at the specimen can be varied to produce junction photocurrents over the range from about 10 pA to about 0.1 mA.

Silicon at room temperature is almost transparent to the 1.15-μm infrared radiation from the second laser; the characteristic penetration depth of this radiation is about 1 cm.[5] The infrared laser is used for three classes of measurements: 1) examination of the silicon-header interface; 2) device temperature profiling; and 3) examination of the device through the backside of the silicon chip. Each of these applications makes use of the penetrating nature of the radiation. In the first application, the reflected-light circuit is used to look through the silicon wafer and observe irregularities at the silicon-header interface in the "flying-spot microscope" mode. The second application makes use of the temperature sensitivity of the silicon absorption; a larger signal is produced on the display screen for those device portions which are warmer than others. Utilizing this sensitivity, one has an electronic technique for thermal mapping of devices which appears to have a number of advantages over the more traditional methods.[6] The third application uses the penetrating infrared radiation to photogenerate carriers deep within silicon devices; this capability allows the operation of devices that are bonded face down (e.g., beam lead devices) to be examined.

Mapping of Device Electrical and Thermal Characteristics

Figure 3 shows photographs of the metallization pattern of a type 2N4431 UHF transistor. This widely available type is designed to furnish 5 W at frequencies up to 1 GHz. There are four in-line cells electrically connected in parallel; these are shown in the left photograph. The total active area of the transistor is a rectangle 1.2 mm long and 0.15 mm wide. The emitter

and base fingers are interdigitated with the emitter fingers coming in from the right, and the base fingers coming in from the left. The finger metallization is 2 μm in width, and the stripe separation is 8 μm. The metal stripe separation allows the active device regions to be accessible to laser irradiation. For the results that will be shown, the devices were scanned while they were connected and biased in the common-emitter configuration. The signal for the display screen was taken from a 60 ohm resistor which served as the collector load. For several of the transistors, it was found that regions of high temperature, so-called "hot-spots," would form within the acceptable operating range listed in the manufacturer's data sheet. This observation was used to aid in understanding the many things the scanner can tell us about the way a device really works. Figure 4 shows photographs of the display screen. The upper left image is the infrared response for a collector-emitter voltage of 26 V and a collector current of 250 mA. The transistor is operating just outside of the hot-spot region. Little of the incident optical energy is absorbed in the device active regions so the display screen signal is weak. The infrared response was actually quite uniform over the device, and the apparent nonuniformity captured in this photograph was due to system noise which had the effect of modulating the presentation of the photoresponse. The lower left photograph was made for the same scanning conditions but with the bias adjusted slightly to put the transistor into hot-spot operation.[6] The region of enhanced photoresponse, the white area, is the hot-spot region as confirmed with the use of a passive infrared microscope. The photoresponse is proportional to the number of electron-hole pairs photogenerated in the device active region. For radiation from the infrared laser, which is lightly absorbed at room temperature, the number of pairs photogenerated increases with temperature because the optical absorption coefficient increases with temperature. This is due primarily to the well-known change in the silicon bandgap with temperature and an increase in the phonon population. It is possible to assign temperature values to this thermal-enhancement of the 1.15-μm response, and a paper describing the details is in preparation.[7]

The upper right photograph is for the same hot-spot conditions, but it was made using the response to the visible laser. Essentially all of the incident light is absorbed in the active regions at room temperature and so no enhancement in the hot-spot is observed.

During normal operation, each laser produces optical radiation at a series of discrete wavelengths centered about the nominal wavelength corresponding to the individual allowed axial modes of the laser. Self-mixing of these wavelengths modulates the light simultaneously at several frequencies. The modulation frequencies are multiples of a fundamental one, and for the particular visible laser used, the light is self-modulated at 500 MHz and 1.0 GHz to a degree adequate for determining the response of devices to light modulated at these frequencies. One inserts a radio receiver between the specimen and the display electronics and tunes the receiver to the selected frequency.

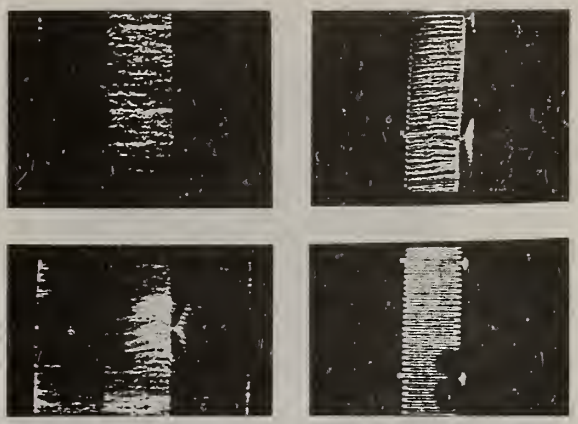

Fig. 4—Electrical responses of microwave transistor. Top left: infrared photoresponse outside the hot-spot regime; bottom left: infrared photoresponse in the hot-spot regime; top right: visible photoresponse in the hot-spot regime; bottom right: visible photoresponse with the modulated light at 500 MHz.

The lower right photograph in Fig. 4 is for the same bias and optical wavelength as for the upper right photograph. In this case the radio receiver is used and the image produced is the response of the transistor to the component of the laser light modulated at 500 MHz. This image is interpreted as the spatial map of the 500-MHz gain of the transistor. It is well known that the hot-spot formation can influence high-frequency device gain.[8] The hot-spot area is revealed quite dramatically, and it can be seen that there are actually two hot spots symmetric about a cell boundary.

By scanning a device with an *electrical* signal applied to its usual input port, one can map on the display screen the regions of the device which are operating nonlinearly at the signal frequency. All that is required is that an i.f. amplifier and detector, tuned to the difference frequency of the electrical signal and a laser mode beat, be inserted between the device output and the display screen.[9] Nonlinearities can indicate stress points and so this mapping may be useful in predicting certain types of device failures. It may also be useful in selecting linear devices for applications in which many devices are used cascaded throughout a communications system; component nonlinearity in such applications is to be avoided since it may produce cross-talk between channels. For these reasons, this unique ability to map device nonlinearities should make the laser scanner invaluable for device design, testing, and reliability.

Internal Operation of Integrated Circuits

The results of scanning a type 7438 dual-input NAND gate IC with 0.633-μm light are shown in Fig. 5. The schematic of the bipolar IC appears in the upper right quadrant along with the truth table. The output transistor (the output is labeled Y) is normally in its high, or

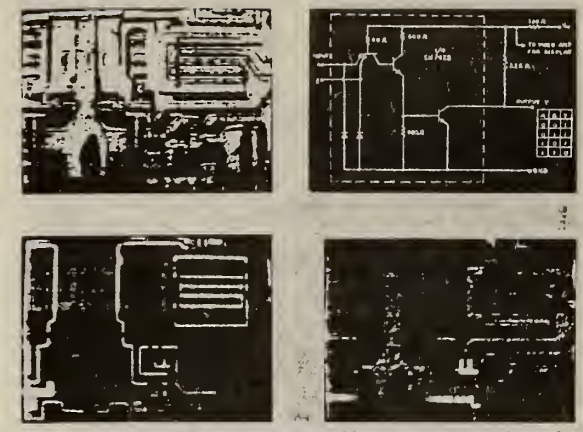

Fig. 5—Type 7438 dual-input NAND gate. Top right: schematic and truth table; top left: reflected-light image; bottom left: photoresponse superimposed on reflected-light image with output in high state; bottom right: photoresponse superimposed on reflected-light image with output in low state.

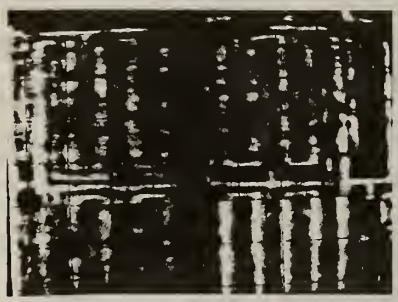

Fig. 6—Photograph of the display when scanning through the back side of a silicon-on-sapphire C-MOS device.

nonconducting state, and to switch it into its low state, i.e., into saturation, requires that both inputs A and B be in their high states. The overall NAND gate operation is specified by the trio of numbers representing A, B, and Y, in that order. As an example, the case in which A and B are high to cause the output to go low is listed in the table as 110. The top left photograph was generated solely by the scanner's reflected light circuit and it shows the metallization. The output transistor occupies the upper right quadrant. To reveal the NAND gate's internal operation, it was biased for normal service with a 330 ohm resistor inserted in the supply bus, and the voltage variation across this resistor during laser scanning modulated the display screen. A transistor operating with significant small-signal current gain will show a large photoresponse and consequently produce a bright image on the display screen. On the other hand, a transistor operating with little small-signal current gain, such as when it is in saturation, will produce almost no image. Thus, from the photoresponse of the elements in the circuit, the different logic states can be deduced. Naturally, changing the state of the NAND circuit yields a new photoresponse display of the active elements.

The photograph in the lower left quadrant of Fig. 5 is the superposition of the scanned IC's electrical response and the reflected-light metallization signal for the 001, 101, and 011 states; all give the same results. The output transistor is in its high state, and an appreciable photoresponse is obtained from portions of the base-collector junction not covered by metallization. The input transistor is located directly below the output transistor, and very little photoresponse is observed from it because no appreciable amplification of the photocurrent generated in the input transistor can occur unless the transistor is out of saturation, i.e., unless both inputs are in their high states.

For the photograph in the lower right quadrant of Fig. 5, the circuit state is 110, and the output transistor is in saturation with little photoresponse obtained from it. The input transistor is out of saturation, and the two L-shaped areas, one under another, below the output transistor are the unobstructed base-collector junction regions around the emitters. The illuminated region to the left is the inter-stage transistor, and the horizontal bar below this is the 4K ohm load for the input transistor.

MOS IC's also have been inspected with the laser scanner. In addition to observing the states of all the logic elements, and the states of the input-output circuits in a shift register, it has been possible to change the state of a desired logic element from 0 to a 1 or vice versa nondestructively with the laser spot.[10] This ability could have far-reaching implications for the testing of LSI circuits, particularly for testing those portions that are embedded, i.e., with no direct connections to external leads.

Examining IC's Through the Wafer

In the work described so far, the scanning light beam was incident on the side of the chip containing the active circuit. But, it is possible to scan a device using penetrating light such that the light enters the back surface and passes almost entirely through the chip before being partially absorbed in the device active region or reflected by the metallization. The 1.15-μm He-Ne laser wavelength is nearly optimum for accomplishing this in silicon devices. Because of the penetration, photocurrents from deep within the chip may contribute to the overall response.

Light scattering due to back surface irregularities must be minimized in order to maintain resolution, and this requires either that the back side be smooth, or that a drop of liquid be placed on the surface having an index of refraction approximately equal to that of the semiconductor.

Back surface scanning was successfully tried on three different types of devices: C-MOS on sapphire, bulk C-MOS, and a bulk bipolar circuit.

The C-MOS on sapphire circuit, a type 4007, was scanned from the back side using visible light ($\lambda = 0.633$ μm) because sapphire is optically transparent. A drop of light oil was deposited on the back of the de-

vice substrate to provide an optically smooth surface. The photograph of the scanner display shown in Fig. 6 was obtained using the reflected light signal mixed with the photoresponse of the inverter. Of the six transistors shown in this figure, only the lower right hand one was electrically connected. The five brightly lit stripes are the gate area of the electrically "on" device.

The bulk silicon C-MOS integrated circuit was also a 4007; however, since the substrate was silicon, it was necessary to use the 1.15-μm wavelength. Figure 7 shows the reflected light image. No oil was needed as the back side was a polished surface.

The third device was a beam-leaded bulk silicon bipolar 709 operational amplifier. In this case oil was deposited on the back of the device die to provide an optically smooth surface. Figure 8a shows the 1.15-μm scanning image obtained when the amplifier was connected to provide a gain of 10 and with 0 V input. The reflected-light signal is superimposed on the photoresponse. Figure 8b shows the device for the same conditions except that the input voltage is now —1.5V, a value sufficiently large to saturate the 709.

These three examples demonstrate a capability of the scanner which can be very useful when metallization on the top of the chip obscures the underlying device active regions but these regions are accessible from the back, or when it is desired to inspect devices bonded into frames or packages "face down" with direct access to the active surfaces blocked by mounting materials.

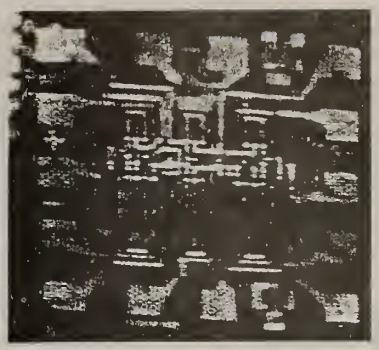

Fig. 7—Photograph of the display when scanning through the back side of a bulk silicon C-MOS device with the infrared laser.

(a)

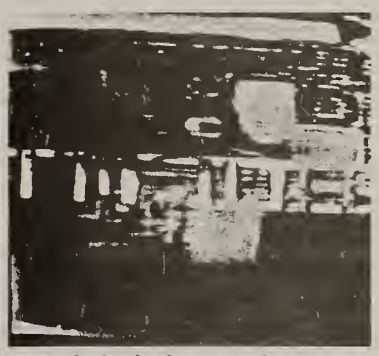

(b)

Fig. 8—Images obtained when scanning a commercial flip-chip operational amplifier with the infrared laser. (a) Input at 0 V. (b) Input at −1.5 V.

Application to Photodetectors and Solar Cells

The laser scanner is an obvious candidate for analyzing photodetector operation. Devices made from a number of materials, including silicon and indium arsenide, and designed for optical communication, have been scanned with unmodulated light, and light modulated at frequencies up to 1.2 GHz, to study gain and spatial response variations. These devices have been both those that utilized internal (avalanche) gain, as well as those which utilized simple photodetection. Even vacuum devices have been scanned; measurements have been made of the uniformity of cathode response for a 931-A photomultiplier to 0.633-μm light modulated at 120 MHz. Experimental solar cells designed for space applications have been laser scanned and the results compared with those obtained with a scanning electron microscope in the electron-beam-induced-current (EBIC) mode. The defects located with the SEM were also found with the laser scanner, in these preliminary experiments. The scanner described in this paper should also be useful in observing variations in solar cell response with light level, and this could be invaluable for cell design. This could be done by scanning the cell with a "small signal" laser while at the same time exposing the cell uniformly to an auxiliary source which would be varied step-wise in intensity.[11]

Summary

The scanner work described makes use of the fact that semiconducting materials are photosensitive as part of their basic nature. Thus, semiconductor devices such as diodes, transistors, and entire integrated circuits made from these materials can be studied using optical radiation. The effect of the optical radiation is to generate electron-hole pairs in a non-damaging way within the specimen. These current-carriers can stimulate device behavior by taking the place of signal current-carriers which are normally supplied by leads fixed to the device. In contrast to signals applied via the leads, which are fixed in position, the optical excitation can be moved

over the surface and within the bulk, and the response of the structures can be studied on a point-by-point basis to learn the inner workings of the device.

In several cases, the scanner has been used to observe device phenomena which one has not been able to study before. The scanner can map the flow of logical information in MOS and bipolar IC's. It can map the operation of transistors at ultrahigh frequencies; it can electronically map the temperature distribution; it can pinpoint the portions of operating devices which are operating in a non-linear manner; and it has the unique ability to look through the back side of silicon chips to observe circuit operation.

References

1. Potter, C. N., and Sawyer, D. E., "A Flying-Spot Scanner," *Rev. Sci. Instrum.* vol. 39, 180-183 (1968).
2. McMahon, R. E., "Laser Tests IC's with Light Touch," *Electronics,* vol. 44, 92-95, (April 12, 1971).
3. Beiser, L., "Laser Beam Scan Enhancement through Periodic Aperture Transfer," *Applied Optics,* vol. 7, 647-650 (1968).
4. Sawyer, D. E., and Berning, D. W., "A Laser Scanner for Semiconductor Devices," NBS Special Publication 400-24, February 1977. Available from the Superintendent of Documents, U.S. Govt. Printing Office, SD Cat. No. C13.10: 400-24.
5. Dash, W. C., and Newman, R., "Intrinsic Optical Absorption in Single-Crystal Germanium and Silicon at 77° and 300°K," *Phys. Rev.*, vol. 99, 1151-1155 (1955).
6. Sawyer, D. E., and Berning, D. W., "Thermal Mapping of Transistors with a Laser Scanner," *Proc. IEEE,* vol. 64, 1634-1635 (1976).
7. Sawyer, D. E., and Lanyon, H. P. D., "Determining Silicon Device Temperatures By Measuring the Thermally-Enhanced 1.15 μm Photoresponse," to be published.
8. Oettinger, F. F., and Rubin, S., "The Use of Current Gain as an Indicator for the Formation of Hot Spots Due to Current Crowding in Power Transistors," *IEEE 10th Annual Proceedings, Reliability Physics,* 12-18 (1972).
9. Sawyer, D. E., and Berning, D. W., "Mapping Nonlinearities Over the Active Regions of Semiconductor Devices," *Proc. IEEE,* vol. 64, 1635-1637 (1976).
10. Sawyer, D. E., and Berning, D. W., "Laser Scanning of MOS IC's Reveals Internal Logic States Non-destructively," *Proc. IEEE,* vol. 64, 393-394 (1976).
11. Lanyon, H. P. D., Worcester Polytechnic Institute, Worcester, MA, private communication.

APPENDIX B

STABILITY OF (THIN FILM) SOLAR CELLS AND MATERIALS

WORKSHOP PROGRAM

Monday, May 1, 1978

8:30 a.m. REGISTRATION

9:15 a.m. WELCOME, PERSPECTIVE, AND WORKSHOP OVERVIEW

9:45 a.m. SESSION I: Status of Present Reliability Testing, Failure Modes, Failure Mechanisms, and Data for Advanced-Cell Materials

Chairman: A. Barnett (Institute for Energy Conversion, U. of Delaware, Newark, DE)

[CdZn]S/Cu_2S
J. D. Meakin and J. E. Phillips (Institute for Energy Conversion, U. of Delaware, Newark, DE)

CdS/Cu-Ternaries
L. Kazmerski (Solar Energy Research Institute, Golden, CO)

Polycrystalline Si
T. L. Chu (Southern Methodist U., Dallas, TX)

COFFEE

MIS and Conducting Oxide/Si
W. Anderson (Rutgers U., Piscataway, NJ)

Conducting Oxide/Si Heterojunctions
R. L. Anderson (Syracuse U., Syracuse, NY)

MIS
S. J. Fonash (Pennsylvania State U., University Park, PA)

1:00 p.m. LUNCH

2:00 p.m. SESSION I (Continued)

AMOS GaAs
R. Stirn (Jet Propulsion Laboratory, Pasadena, CA)

Polycrystalline GaAs
S. Chu (Southern Methodist U., Dallas, TX)

Amorphous Si
D. Carlson (RCA Corp., Princeton, NJ)

COFFEE

SESSION II: Measurements and Tests used to Define Stability in Related Technologies

Chairman: R. I. Scace (National Bureau of Standards, Washington, DC)

Silicon Cell Space Program Experience
P. Iles (Optical Coating Laboratory, Inc., City of Industry, CA)

Concentrator Solar Cells
W. McLevige (Sandia Laboratories, Albuquerque, NM)

5:00 p.m. ADJOURN

6:30 p.m. CASH BAR (Ramada Inn)

7:30 p.m. WORKSHOP DINNER (Ramada Inn)

Tuesday, May 2, 1978

9:15 a.m. SESSION II (Continued)

DoD Experience
J. Adolphson (NASA Goddard Space Flight Center, Greenbelt, MD)

Methods and Tests for Devices at the Bell Telephone Laboratory
C. W. Green (Bell Telephone Laboratories, Allentown, PA)

Power and CMOS Devices
S. Kukumaris (RCA Corp., Somerville, NJ)

COFFEE

Interdiffusion Phenomena
L. Kazmerski (Solar Energy Research Institute, Golden, CO)

Corrosion
R. Frankenthal (Bell Telephone Laboratories, Murray Hill, NJ)

Terrestrial Silicon Array Field and Test Experience
R. Ross (Jet Propulsion Laboratory, Pasadena, CA)

1:00 p.m. LUNCH

2:00 p.m. SESSION II (Continued)

Designing Accelerated Aging Tests for Predicting Array Life
D. Carmichael (Battelle Columbus Laboratories, Columbus, OH)

2:30 p.m. SESSION III: Working Group Sessions — To identify tests and measurement procedures that can be used to enhance the prediction of material and device stability for each of the three solar cell groups.

GROUP 1: [CdZn]S/Cu_2S, CdS/Cu-Ternaries, CdS/InP, and Amorphous Si
Chairman: L. Kazmerski (Solar Energy Research Institute, Golden, CO)
Location: Green Auditorium

GROUP 2: Polycrystalline Si, MIS, and Conducting Oxide Si
Chairman: J. Shewchum (McMaster U., Hamilton, Ontario)
Location: Lecture Room A

GROUP 3: Polycrystalline and AMOS GaAs
Chairman: R. Stirn (Jet Propulsion Laboratory, Pasadena, CA)
Location: Lecture Room D (n.b.: Wednesday, Group meets in Employee's Lounge)

5:00 p.m. ADJOURN

Wednesday, May 3, 1978

9:15 a.m. SESSION III (Continued)

GROUP 1: [CdZn]S/Cu_2S, CdS/Cu-Ternaries, CdS/InP, and Amorphous Si
Chairman: L. Kazmerski (Solar Energy Research Institute, Golden, CO)
Location: Green Auditorium

GROUP 2: Polycrystalline Si, MIS, and Conducting Oxide Si
Chairman: J. Shewchum (McMaster U., Hamilton, Ontario)
Location: Lecture Room A

GROUP 3: Polycrystalline and AMOS GaAs
Chairman: R. Stirn (Jet Propulsion Laboratory, Pasadena, CA)
Location: Employee's Lounge

10:50 a.m. COFFEE

11:20 a.m. TOUR (Selected Energy-Related Projects of NBS)
Tour is for all participants not involved in the preparation of working group summaries for presentation in Session IV.

1:00 p.m. LUNCH

2:00 p.m. SESSION IV: Working Group Presentations of Summaries and Recommendations
Chairman: H. A. Schafft (National Bureau of Standards, Washington, DC)

3:30 p.m. SESSION V: Closing Remarks
Chairman: D. E. Sawyer (National Bureau of Standards, Washington, DC)

4:00 p.m. ADJOURN

CREDITS:

Workshop Sponsor:

Advanced Materials R&D Branch
Division of Solar Technology
Department of Energy

Steering Committee:

Allen Barnett
University of Delaware

Gordon Gross
Solar Energy Research Institute

Gary Jones
Sandia Laboratories

J. W. Lathrop
Clemson University

L. M. Magid
Department of Energy

Joseph M. Morabito
Bell Telephone Laboratories

Ronald Ross
Jet Propulsion Laboratory

R. J. Stirn
Jet Propulsion Laboratory

Brown Williams
David Sarnoff Laboratories

Organizing Committee:

Donald L. Feucht
Department of Energy

David E. Sawyer
National Bureau of Standards

Harry A. Schafft
National Bureau of Standards

NBS Workshop Committee:

Chairman - David E. Sawyer
Coordination - Harry A. Schafft
Registration - Elaine C. Cohen
Arrangements - Sara R. Torrance, JoAnn Lorden, Elaine C. Cohen

APPENDIX C

PHOTOVOLTAICS MATERIAL AND DEVICE MEASUREMENTS WORKSHOP

Preliminary Plans

Dates June 11-13, 1979

Location Stouffer's National Center Hotel
2399 Jefferson Davis Highway, Arlington, VA 22202

Sponsor Solar Energy Research Institute in cooperation with NBS

Purpose

To accelerate the development of thin-film solar cells by improving the versatility and reliability of material and device measurement techniques.

Objectives

1. Identify and discuss the techniques which have been used to measure selected key properties of thin-film polycrystalline materials and devices.

2. Discuss the applicability of these techniques to the understanding of thin-film polycrystalline materials and devices.

3. Identify measurement techniques which require improvements.

4. Identify new measurement techniques.

5. Suggest methods for achieving:

   - more meaningful material and device measurements
   - greater measurement reproducibility
   - greater efficiency in the development and fabrication of thin-film devices
   - greater confidence in comparing and evaluating thin-film device measurements.

6. Foster greater communication between device researchers and measurement methods experts.

Program

The workshop will have three sessions devoted to formal presentations, a general discussion session, and an evening poster session for informal presentations. David Sawyer of NBS, and Joseph M. Morabito of Bell Labs, will serve as co-chairmen for the workshop.

The sessions will be designed to achieve the objectives stated above; however, thin-film amorphous materials and devices will not be included in this workshop.

Each session will be organized and conducted by a set of co-chairmen. The following have agreed to serve as session co-chairmen:

Structural/Chemical Session
John D. Meakin, University of Delaware
Fritz Wald, Mobil-Tyco

Optical/Electro-Session
Lewis M. Frass, Chevron Research Company
Alan Fahrenbruch, Stanford University

Charge Transport Session
P. Daniel Dapkus, Rockwell International
H. H. Weider, Naval Ocean Systems Center

Poster Session
L. L. Kazmerski, SERI
Steve Hogan, SERI

Discussion Session
David Sawyer, NBS
Joseph M. Morabito, Bell Laboratories

Each session will have one invited keynote speaker whose presentation will be scheduled for 45 minutes (35-minute presentation; 10-minute question and answer period). This will be followed by several invited contributed papers which are scheduled for 40 miutes (20-minute presentation; 10-minute question and answer period). Papers solicited through a call for papers will be used to fill in each session or be scheduled for the poster session.

Documentation

Four weeks prior to the workshop all presenters will be required to submit an extended abstract (two-page maximum). The abstracts will be compiled, printed and distributed at the meeting. Specific requirements for the content of the abstracts will be defined by the co-chairmen for each session.

Following the workshop a proceedings will be mailed to all registrants and distributed through TIC and NTIS. The proceedings will include the extended abstracts, viewgraphs, and written questions and answers from each presentation.

APPENDIX D

Publications and Talks

D.1 Recent Publications:

Sawyer, D. E., A Technique for Using An Optical Scanner to Reveal Solar Cell Defects, *Proc. 13th IEEE Photovoltaic Specialists Conf.*, Washington, D.C., June 5-8, 1978, pp. 1249-1250 (1978).

Sawyer, D. E., Kessler, H. K., and Schafft, H. A., Measurement Techniques for Solar Cells, Quarterly Report, September 15 to December 31, 1977, NBSIR 78-1488 (July 1978).

Sawyer, D. E., Kessler, H. K., and Schafft, H. A., Measurement Techniques for Solar Cells, Quarterly Report, January 1 to March 31, 1978, NBSIR 78-1513 (September 1978).

Sawyer, D. E., Kessler, H. K., and Schafft, H. A., Solar Cell Measurement Technique Development and Other Services, *Proc. DoE Annual Review for Advanced Materials R&D Branch,* Vail, Colorado, October 24-26, 1978, pp. 41-50 (January 1979).

D.2 Publications in Press

Sawyer, D. E., Kessler, H. K., and Schafft, H. A., Measurement Techniques for Solar Cells, Quarterly Report, April 1 to June 30, 1978, NBSIR 78-1488 (July 1978).

Semiconductor Measurement Technology: NBS/DOE Workshop, Stability of (Thin Film) Solar Cells and Materials, D. E. Sawyer and H. A. Schafft, Editors, NBS Special Publication 400-58 (August 1979).

D.3 Talks

Sawyer, D. E., A Technique for Using An Optical Scanner to Reveal Solar Cell Defects, Proc. 13th IEEE Photovoltaic Specialists Conf., Washington, D.C., June 5-8, 1978.

Sawyer, D. E., Kessler, H. K., and Schafft, H. A., Solar Cell Measurement Technique Development and Other Services, Proc. DoE Annual Review for Advanced Materials R&D Branch, Vail, Colorado, October 24-26, 1978.

Sawyer, D. E., Solar Cell Laser Scanning, invited talk and seminar, Institute of Energy Conversion, University of Delaware, November 10, 1978.

NBS-114A (REV. 9-78)

U.S. DEPT. OF COMM. BIBLIOGRAPHIC DATA SHEET	1. PUBLICATION OR REPORT NO. NBSIR 80-2027	2. Gov't. Accession No.	3. Recipient's Accession No.

4. TITLE AND SUBTITLE

Measurement Techniques for Solar Cells: Annual Report for the Period September 15, 1977 to December 14, 1978

5. Publication Date: July 1980

6. Performing Organization Code

7. AUTHOR(S)

D. E. Sawyer, H. K. Kessler, and H. A. Schafft

8. Performing Organ. Report No.

9. PERFORMING ORGANIZATION NAME AND ADDRESS

NATIONAL BUREAU OF STANDARDS
DEPARTMENT OF COMMERCE
WASHINGTON, DC 20234

10. Project/Task/Work Unit No.

11. Contract/Grant No.: Task Order A054-SE

12. SPONSORING ORGANIZATION NAME AND COMPLETE ADDRESS (Street, City, State, ZIP)

Advanced Materials R&D Branch
Division of Distributed Solar Technology
Department of Energy
20 Massachusetts Ave., N.W., Washington, D. C. 20545

13. Type of Report & Period Covered: Interim Report/Sep. 15, 1977-Dec. 15, 1978

14. Sponsoring Agency Code

15. SUPPLEMENTARY NOTES

☐ Document describes a computer program; SF-185, FIPS Software Summary, is attached.

16. ABSTRACT (A 200-word or less factual summary of most significant information. If document includes a significant bibliography or literature survey, mention it here.)

This is a report of work in a program on solar cell measurement technique development and other services which was performed at NBS in September 15, 1977 to December 14, 1978. The objectives of the program are to assist the DOE thin film photovoltaic effort by developing solar cell device and material measurement techniques using the NBS-developed laser flying-spot scanner, by assisting DOE in organizing and hosting appropriate workshops and symposia, and by providing general consultation and liaison service.

A technique was developed which employs forward biasing during laser scanning of the solar cell to reveal defects including cracks, metallization breaks, and regions of metallization not in ohmic contact with the underlying semiconductor. The technique also has provided information useful to cell designers. The experimental results obtained are consistent with predictions made by a first-order theory developed in-house, and by subsequent mathematical modelling performed by the University of Southern California under subcontract. Single-crystal silicon artifacts have been designed to couple laser scanning measurements with mathematical analyses to define quantatively the capabilities of the laser scanner techniques to detect cell defects and spatial nonuniformaties of cell performance.

The laser scanner was designed originally to analyze integrated circuit devices. A number of scanner modifications were made and ancillary apparatus was developed to adapt the scanner for examining solar cells. These modifications include an increase in the specimen area that can be scanned without specimen repositioning, the use of a more efficient means of electronically coupling scanned cells to the display electronics, and the construction of a high-intensity source for light-biasing cells during scanning.

A workshop on Stability of (Thin Film) Solar Cells and Materials was held May 1-3, 1978 at NBS, Gaithersburg, MD. Plans were initiated for a workshop on photovoltaic material and device measurements scheduled to be held in the Washington, D. C. area in the spring of 1979.

17. KEY WORDS (six to twelve entries; alphabetical order; capitalize only the first letter of the first key word unless a proper name; separated by semicolons)

Device measurements; laser scanning; light-biasing; metallization; ohmic contacts; reliability; semiconductor measurements; sheet resistance; solar cell; solar cell measurements; solar cell stability.

18. AVAILABILITY

[X] Unlimited

☐ For Official Distribution. Do Not Release to NTIS

☐ Order From Sup. of Doc., U.S. Government Printing Office, Washington, DC 20402, SD Stock No. SN003-003-

[X] Order From National Technical Information Service (NTIS), Springfield, VA. 22161

19. SECURITY CLASS (THIS REPORT)	21. NO. OF PRINTED PAGES
UNCLASSIFIED	68
20. SECURITY CLASS (THIS PAGE)	22. Price
UNCLASSIFIED	$7.00

USCOMM-DC